






Article

Scatter Search for Optimal Sizing of a Hybrid Renewable Energy System for Scheduling Green Hydrogen Production

Andrés Cacereno ^{1,*}, Begoña González Landín ¹, Antonio Pulido ¹, Gabriel Winter ¹
and José Andrés Moreno ²

¹ Instituto Universitario de Sistemas Inteligentes y Aplicaciones Numéricas en Ingeniería, Universidad de Las Palmas de Gran Canaria, 35017 Las Palmas de Gran Canaria, Spain; bego.landin@ulpgc.es (B.G.L.); antonio.pulido@ulpgc.es (A.P.); gabriel.winter@ulpgc.es (G.W.)

² Instituto Universitario de Desarrollo Regional, Universidad de La Laguna, 38071 La Laguna, Spain; jamoreno@ull.edu.es

* Correspondence: andres.cacereno@ulpgc.es

Abstract: At present, energy demands are mainly covered by the use of fossil fuels. The process of fossil fuel production increases pollution from oil extraction, transport to processing centers, treatment to obtain lighter fractions, and delivery and use by the final consumers. Such polluting circumstances are aggravated in the case of accidents involving fossil fuels. They are also linked to speculative markets. As a result, the trend is towards the decarbonization of lifestyles in advanced societies. The present paper addresses the problem of the optimal sizing of a hybrid renewable energy system for scheduling green hydrogen production. A local system fully powered by renewable energies is designed to obtain hydrogen from seawater. In order to monetize excess energy, the grid connection of the system is considered under realistic energy market constraints, designing an hourly purchasing strategy. This crucial problem, which has not been taken into account in the literature, is solved by the specific dispatch strategy designed. Several optimization methods have been used to solve this problem; however, the scatter search method has not previously been employed. In this paper, the problem is faced with a novel implementation of this method. The implementation is competitive in terms of performance when compared to, on the one hand, the genetic algorithm and differential evolution methods, which are well-known state-of-the-art evolutionary algorithms, and, on the other hand, the optimal foraging algorithm (OFA), a more recent algorithm. Furthermore, scatter search outperformed all other methods in terms of computational cost. This is promising for real-world applications that require quick responses.

Keywords: green hydrogen; optimization; scatter search; evolutionary algorithms; dispatch strategy

MSC: 90C59; 68W50



Citation: Cacereno, A.; González Landín, B.; Pulido, A.; Winter, G.; Moreno, J.A. Scatter Search for Optimal Sizing of a Hybrid Renewable Energy System for Scheduling Green Hydrogen Production. *Mathematics* **2024**, *12*, 3848. <https://doi.org/10.3390/math12233848>

Academic Editor: Hua Ke

Received: 24 October 2024

Revised: 24 November 2024

Accepted: 3 December 2024

Published: 6 December 2024



Copyright: © 2024 by the authors. Licensee MDPI, Basel, Switzerland. This article is an open access article distributed under the terms and conditions of the Creative Commons Attribution (CC BY) license (<https://creativecommons.org/licenses/by/4.0/>).

1. Introduction

The more developed societies become, the greater the increase in energy demand. Currently, this demand is mainly met by the use of fossil fuels. Fossil fuels are limited resources linked to both economic and availability uncertainties. They also have undesirable climatic effects. These factors bring to light the vulnerability of energy markets and the non-sustainability of energy systems. In order to manage such circumstances, the governments of many countries are promoting the transition to clean energy. For decades, around 80% of the global energy mix has been supplied by fossil fuels. This percentage will drop below 75% by 2030 and will be slightly above 60% by 2050 [1].

In order to meet this demand, various renewable energy sources are currently being employed to support traditional energy sources such as solar photovoltaic, wind, geothermal, and marine energy. The technologies to obtain energy from the sun and wind are

particularly mature [2,3]. However, unpredictable changes in nature have an impact on energy production. Therefore, energy storage systems are necessary to overcome this issue.

Hydrogen is considered an energy carrier, because of its ability to store energy, which can be retrieved when needed. The energy contained in hydrogen can be more than twice that contained in petroleum derivatives. Hence, many countries are turning their attention to hydrogen as an alternative to fossil fuels. However, hydrogen is not naturally present in our environment. It is present as a mixture with other elements, such as oxygen in the case of water or carbon in the case of hydrocarbons. It takes a lot of energy to dissociate hydrogen and oxygen from water. When such energy is obtained from renewable energy sources, the term green hydrogen is used because of the lack of carbon emissions into the atmosphere.

The motivations of this research were twofold. On the one hand, we aimed to demonstrate that the Canary Islands have the ideal conditions to produce green hydrogen and, therefore, to collaborate in the decarbonization of an isolated energy system and, on the other hand, to test a novel implementation of the scatter search method, which provides a novel procedure to combine solutions. In the present paper, several scenarios are considered for designing the main components of a grid-connected plant to schedule the production of hydrogen from renewable energy sources. A dispatch strategy is designed and explored to evaluate these scenarios. This dispatch strategy takes into account the connection to the grid to deliver excess energy under the constraints of the energy market. The evolutionary approach provided by scatter search is used to solve this problem. The main contributions of this paper are described below:

- The optimal sizing of a grid-connected hybrid renewable system with hydrogen technologies is addressed, while several optimization techniques are applied. A novel implementation of scatter search is applied in the present study and its performance is compared with methods obtained from the literature. In addition, scatter search has not previously been used to solve this kind of problems. Both the novel implementation and its use in an unexplored field permit a broader understanding of the method.
- Renewable system alternatives are designed using climatological data, which are obtained from Copernicus [4]. Copernicus is the Earth observation component of the European Union's Space Programme. It offers information services that draw from satellite Earth Observation and in situ (non-space) data.
- The optimal sizing is addressed to meet the scheduled hydrogen demand. The dispatch strategy designed allows excess energy to be delivered to the grid according to market constraints. Considering such realistic constraints avoids oversizing the energy system.

This paper is organized as follows: Section 2 explores the related literature. Section 3 introduces the materials and methods. It includes the proposed system layout, the mathematical modeling of the main devices, the problem formulation, the optimization process, and the scope of the experiment. Section 4 displays the results. Section 5 provides a discussion. Finally, Section 6 gives the conclusions.

2. Literature Review

This is followed by a review of the literature, in order to expose some of the identified gaps that this study addresses.

2.1. Optimal Sizing of Hybrid Renewable Energy Systems

Many authors have studied the optimal sizing of hybrid renewable energy systems. The main objective consists of determining the dimensions of system devices, while economic and technical indicators are taken into account. Katsigiannis and Georgilakis [5] used simulated annealing and Tabu search to optimize a small autonomous power system with minimal energy cost. The system contained wind turbines, photovoltaic panels, a diesel generator, a biodiesel generator, fuel cells, and batteries. Alshammari and Asumadu [6]

studied the optimal design of a hybrid renewable energy system considering wind, photovoltaic, biomass, and battery technologies. Harmony search, Jaya, and particle swarm optimization algorithms were used to meet the electricity demand in a cost-effective, efficient, and reliable manner. Maleki et al. [7] applied an improved harmony search algorithm for optimal sizing of a hybrid system based on solar photovoltaic and battery storage units. Fares et al. [8] solved the optimal sizing of a hybrid energy system based on photovoltaic installations, wind turbines and battery storage. The performance of several metaheuristics was compared. He et al. [9] proposed a hybrid electrical-thermal energy storage system for optimal sizing of a renewable hybrid system based on photovoltaic panels and wind turbines. They employed particle swarm optimization as an optimization method. Saha et al. [10] optimized the size of a photovoltaic-, biomass-, and battery-based hybrid system to electrify an isolated village. They employed the discrete gray wolf optimization algorithm to minimize the net present cost under technical, social, and economic constraints. These references considered the use of batteries as energy storage systems, which are widely employed to this end [11]. However, they are not recommended for long-term operations [12].

2.2. Optimal Sizing of Hybrid Renewable Energy Systems with Hydrogen Technologies

Focusing on promising alternatives for energy storage, many efforts have been centered on optimizing the size of energy systems based on renewable sources and hydrogen technologies. For this purpose, several optimization techniques have been used, which can be classified as classical, software simulation tools, and modern techniques. Classical optimization includes methods such as mixed integer programming [13] or iterative methods [14]. The complexity of the problem to be solved influences the classical techniques.

In terms of software simulation tools for the design of renewable systems, HOMER, (Hybrid Optimization Model for Electric Renewables) is the most widely used. Lacko et al. [15] considered a system based on solar photovoltaic arrays and wind turbines that included hydrogen technologies to achieve the lowest total net present cost. Das et al. [16] analyzed the feasibility of systems based on photovoltaic, battery, and fuel cells to minimize the total net present cost and cost of energy. Duman and Güler [17] studied the energy cost of systems based on solar photovoltaic arrays and wind turbines, including hydrogen technologies. Such tools are very useful when designers do not require exhaustive control of the optimization process. Numerous studies have been conducted in which modern techniques were applied and a customized optimization process was developed. Mohseni et al. [18] optimized the size and typology of the components of an isolated microgrid system with hydrogen technologies. They proposed a metaheuristic-based approach, which was compared with several metaheuristics to reduce the total net present cost. Siddiqui and Dincer [19] optimized a renewable energy system to produce electricity, hydrogen, and ammonia based on solar photovoltaic panels and wind turbines. A genetic algorithm was used to obtain minimum cost rates and the maximum energy efficiency. Sun et al. [20] used the whale optimization algorithm for the optimal design of a hybrid photovoltaic, biowaste, and fuel cell system based on hydrogen energy storage. They minimized the total net present cost under reliability constraints. El-Sattar et al. [21] addressed the optimal size of an isolated hybrid system to meet electricity demand with a cost improvement. The main configuration of the system included biomass, photovoltaic modules, electrolyzer units, hydrogen tank units, and a fuel cell system. They used the mayfly optimization algorithm (MOA) to meet the demand with the lowest energy cost and greenhouse gas emissions. Elnozahy et al. [22] proposed an electrical/green hydrogen generation system based on photovoltaic, battery, and hydrogen technologies. They employed particle swan optimization, taking into account the levelized cost of energy, the net present cost, and the capability to meet the demand. Hou et al. used various modified harmony search algorithms for the sizing of a standalone solar-hydrogen system in green buildings. The objective function was based on the probability of loss of power supply and the annual cost of the system. Güven and Mengi [23] developed a comparison of several metaheuristic algorithms for the

sizing of an isolated hybrid energy system. They proposed an atom search optimization algorithm, which outperformed all other algorithms. They considered the annual cost of the system as the main criterion during the optimization process. Phan-Van et al. [24] designed a microgrid based on photovoltaic, electrolyte, fuel-cell, battery, and hydrogen technologies. Several metaheuristic optimization algorithms were employed. The particle swarm optimization algorithm outperformed the other methods. In these cases, isolated systems were designed to meet the demand.

The most commonly studied hybrid renewable systems are those separated from the grid (off-grid). In these cases, the excess energy flux is wasted once the energy storage systems are full. Moreover, isolated systems cannot import energy when needed. When hybrid renewable systems are connected to the grid (on-grid), excess energy flux can be leveraged and energy shortages covered. An extensive review on hydrogen and grid connection was developed by Irham et al. [25]. Several studies have considered the optimal sizing of grid-connected renewable hybrid systems with hydrogen technologies. In this sense, Garcia-Trivino et al. [26] sized a grid-connected hybrid system including solar photovoltaic arrays, wind turbines, batteries, and hydrogen technologies. Gharibi and Askarzadeh [27] studied the optimization of a hybrid system connected to the grid based on solar photovoltaic arrays, wind turbines, a diesel generator, and hydrogen technologies. They introduced a grid factor as a decision variable to optimize the amount of electricity sold. Okundamiya [28] demonstrated the size optimization of a grid-connected hybrid system based on photovoltaic and fuel cells. The system was designed to avoid power loss at certain times due to the connection to an unreliable grid. Le et al. [29] presented the optimization of the design and operation of a grid-connected hybrid energy system based on photovoltaic, battery, and hydrogen technologies. The connection to the grid allowed energy to be imported when needed. Not taking energy from the grid is a requirement for the production of green hydrogen. Therefore, in the present study, the grid connection was considered exclusively to provide energy. The reality of complex energy systems does not allow the full excess flux to be leveraged from on-grid renewable systems. Hour by hour, energy companies declare the energy that they can accept from each renewable energy source, which is an aspect that is normally underestimated.

2.3. Scatter Search to Solve Engineering Optimization Problems

Scatter search (SS) [30] is an evolutionary algorithm for optimization, in which a moderately sized set of solutions evolves due to intelligent mechanisms of combination and selection. Unlike the usual strategies in evolutionary optimization, the search for a local optimal solution is a guided task. The basic concepts and principles of SS arose in the 1970s, based on strategies combining decision rules and constraints [31]. However, scatter search remains an object of research. Like any other metaheuristic, scatter search can have a good performance for some problems or instances, and not such a good performance for others. Advances in its application can be achieved in two main directions. On the one hand, by exploring its application to types of problems where it has not been tested, thus broadening the field of successful applications. On the other hand, by making the necessary adjustments so that the performance improves and can be competitive with the state-of-the-art procedures in a specific field of application.

Scatter search is an evolutionary metaheuristic that, unlike most evolutionary metaheuristics such as differential evolution, does not work with a large population of solutions that evolve in the search space, but with a moderately sized set of solutions called the "Reference Set". Here, we are talking about a reference set of no more than 10, 15, or 20 solutions, instead of a population of hundreds, or even thousands. Another distinctive feature of scatter search is that the role of randomness is reduced in the combination of evolving solutions to obtain new solutions that improve the exploration and exploitation capacity of the metaheuristic. Thus, instead of making many combinations to take advantage of only the most promising combinations, the aim is to select and combine those solutions that can lead to significant improvements in the quality and diversity of the reference set itself.

In addition, the combination of solutions also tries to reduce the role of randomness by allowing the combinations to take advantage of the good characteristics of the combined solutions. Finally, in order to maintain a reference set that is composed of both high-quality solutions and essentially different solutions, the resulting combinations or their improvements through local searches are incorporated into the reference set for two reasons. On the one hand, because they consist of higher-quality solutions than those already included in the reference set, or because, without neglecting quality, they give a greater degree of dispersion to the reference set, while keeping its size limited.

The metaheuristic SS works as follows. In order to create a population of solutions, a reference set of moderate size is generated. This set evolves to intensify and diversify the search based on its solutions. Some solutions of the reference set are combined, and a local search procedure is applied to the resulting solutions. Then, the reference set is updated by including both the good and dispersed solutions obtained. These steps are repeated until no improvement is obtained or another stopping condition is met [30]. Scatter search (SS) has been successfully applied to solve complex optimization problems [32]. In Silva et al. [33], the simultaneous optimization of fuel emission and cost objectives was explored by developing an improved SS. Tan et al. [34] applied SS to address a scheduling problem to optimize an energy-efficient continuous steelmaking casting process. Pérez Posada et al. [35] used the SS heuristic for the optimal location, sizing, and contract pricing of distributed generation in electric distribution systems. Stojiljkovic et al. [36] employed SS to solve a multi-objective bi-level optimization problem regarding the design and operation of an energy supply system. However, SS has never been used for the optimal sizing of energy systems based on renewable sources and hydrogen technologies. In addition, the scatter search implementations used by the authors of the present research combine two solutions to achieve a new one. The novel implementation in the present research consists of combining a scaled difference of two solutions with a third solution, which provides good performance, as demonstrated.

In the present paper, this method is explored and its results are compared with those obtained from the use of differential evolution [37], the genetic algorithm proposed by Holland [38], and the optimal foraging algorithm (AFO). Both differential evolution and the genetic algorithm are well-known and well-regarded among the state-of-the-art of evolutionary methods. Differential evolution was designed as a stochastic direct search method that uses a vector population. Information from the vector population is employed to alter the search space. Differential evolution has been used to solve the optimal sizing of energy systems based on renewable sources. Ramli et al. [39] applied a multiobjective differential evolution algorithm for the sizing optimization of a solar, wind, and diesel hybrid microgrid system with battery storage. Yang and Le [40] developed a techno-economic optimization of a standalone system based on solar, wind, and battery. To solve the problem, they proposed a multi-objective differential evolution algorithm. In addition to considering hydrogen technologies, Abedi et al. [41] employed differential evolution to solve mixed integer non-linear optimization problems by considering a hybrid photovoltaic/wind/fuel cell energy system. In their research, the differential evolution outperformed another well-known evolutionary method (particle swarm optimization). The genetic algorithm proposed by Holland was the first population-based method. Mimicking the natural processes of genetic variation and inheritance, the population evolves through a series of operators, such as selection, reproduction, and mutation [42]. Nagapurkar and Smith [43] developed a techno-economic optimization of a microgrid using genetic algorithm to minimize the levelized cost of energy. The optimal foraging algorithm [44] was tested by the authors on a benchmark and compared to several methods. The algorithm proved to be very competitive; however, it has not been used to solve the problem addressed in this research. Optimization with evolutionary algorithms can be an unfeasible approach for solving real-world engineering problems, due to the high computational cost. In this sense, SS can be a less costly method.

Therefore, some gaps in the state of the art concerning the optimal sizing of energy systems based on renewable sources and hydrogen technologies have been identified. These are dealt with in this paper.

3. Materials and Methods

This section presents the proposed energy system, as well as the mathematical modeling of its constituent devices and the formulation of the optimization problem. Then, the optimization process is detailed, including the dispatch strategy developed and the scatter search implementation proposed. In addition, the scope of the experimentation is given.

3.1. System Layout

This study proposes an energy system based on renewable sources and hydrogen technologies. The system basically consists of solar photovoltaic panels (PV), wind turbines (WT), a battery bank, an electrolyzer, and a hydrogen tank (H₂ TANK). An inverter (INV) is used to transform the energy coming from the photovoltaic solar panels, and a converter (CON) is used to transform the energy related to the battery bank. The main components of the system are shown in Figure 1.

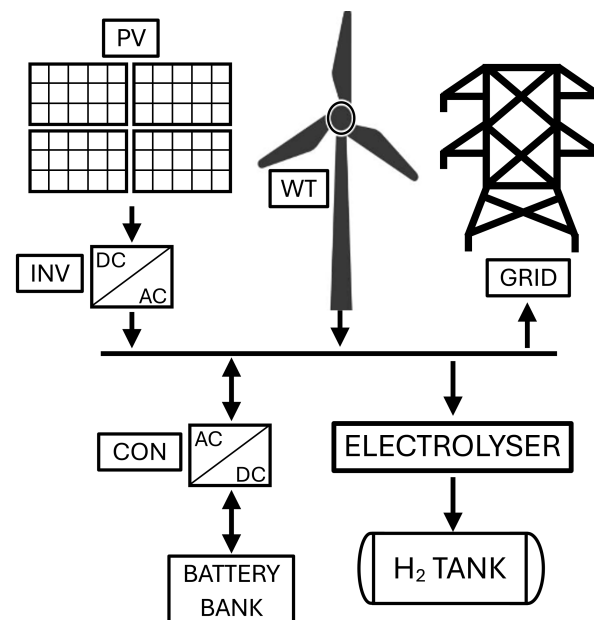


Figure 1. Hybrid system configuration layout.

Basically, energy from renewable sources powers the system. Since alternating current (AC) is needed, an inverter is used to transform power from the solar photovoltaic panels. Therefore, power is transformed from direct current (DC) to alternating current (AC). The power from wind turbines does not need to be transformed. This power feeds an electrolyzer, which produces hydrogen from water. The hydrogen produced is stored in a tank. A battery bank is used to store excess power or to supply power to the electrolyzer when the energy from renewable sources is not sufficient. The power going to the battery bank must be transformed to direct current (DC) by the converter. In Figure 1, the grid connection of the system can be seen. When the battery bank is full of charge, excess power can be delivered to the grid. In order to ensure the green production of hydrogen, power is not taken from the grid. The mathematical models used are detailed below.

3.2. Mathematical Modeling of System Units

This subsection describes the mathematical modeling of the main units of the system.

3.2.1. Photovoltaic Modules

Light energy is converted into electrical energy by photovoltaic modules. Before calculating the generated power, the temperature of the cell must be evaluated. In the present study, Equations (1) and (2) are employed to determine the cell temperature at time ($T_C(t)$) and to compute the expected power output of a photovoltaic module at time ($PV_p(t)$), respectively [7].

$$T_C(t) = I(t) \left(\frac{T_{NOCT} - 20}{800} \right) + T_A(t) \tag{1}$$

$$PV_p(t) = P_{R,PV} \left(\frac{I(t)}{R_{REF}} \right) (1 + \delta_T(T_C(t) - T_{REF})) \tag{2}$$

where $I(t)$ is the irradiance at time, T_{NOCT} is the cell temperature at normal operating conditions (45 °C), $T_A(t)$ is the ambient temperature at time, $P_{R,PV}$ is the rated power of the panel (500 W), R_{REF} is the reference solar radiance, δ_T is the temperature coefficient of the maximum power of the photovoltaic modules (−0.0037), and T_{REF} is the reference temperature of the solar cell (45 °C). In order to transform solar power, an inverter is used (inverter efficiency $\eta_{inv} = 0.965$).

3.2.2. Wind Turbines

Wind energy is converted into electrical energy by employing wind turbines. Following the power law in Equation [45], the wind speed captured at the height of the measuring device must be converted to the height of the hub (see Equation (3)).

$$\frac{v_h}{v_r} = \left(\frac{h_h}{h_r} \right)^{\alpha_1} \tag{3}$$

where v_r is the wind speed at the reference height h_r , v_h is the wind speed at the height of the hub h_h (55 m), and α_1 is the friction coefficient (0.14 m). The power output of the wind turbine considered for the study ($P_{WT} = 660$ kW) follows the power curve provided in Figure 2. It can be seen that the wind turbine does not operate at wind speeds below 4 m/s or above 25 m/s.

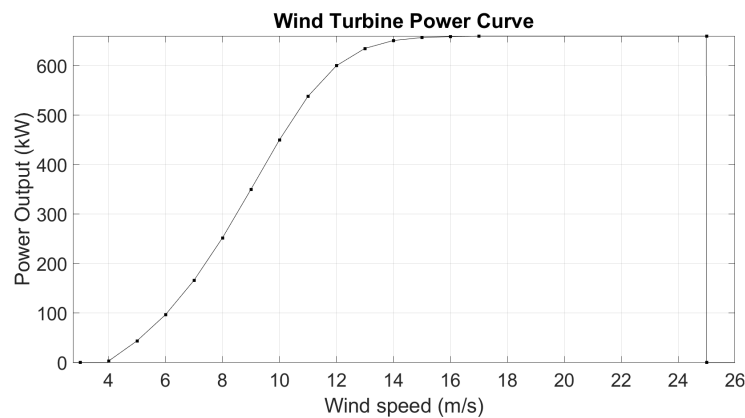


Figure 2. Wind turbine power curve.

3.2.3. Battery Bank

The non-constant nature of renewable sources implies that energy is not guaranteed. Therefore, it is necessary to use a battery bank to supply power to the electrolyzer. In addition, excess energy from renewable sources can be stored in a battery bank. The bank’s capacity (C_{BAT}) is designed to satisfy the electrolyzer for a determined number of hours (NH). This is calculated using Equation (4) [46].

$$C_{BAT} = \frac{C_{ELE} \cdot NH}{DOD \cdot \eta_{BAT} \cdot \eta_{CONV}} \quad (4)$$

where C_{ELE} is the electrolyzer's capacity, NH is the number of hours of autonomy of the battery bank, DOD is the depth of discharge (80%), η_{BAT} is the battery bank's efficiency (96%), and η_{CONV} is the converter's efficiency (95%).

On the one hand, the battery bank can supply power to the electrolyzer when the renewable energy is insufficient. However, the battery bank can store excess energy when the renewable energy exceeds the capacity of the electrolyzer. In order to verify that the capacity of the battery bank is not exceeded, the virtual state of charge (VSOC) must be calculated as shown in Equation (5).

$$VSOC = P_{BAT_0}(1 - \alpha_2) + \left(P_{REN} - \left(\frac{P_{ELE}}{\eta_{ELE}} \right) \right) \eta_{CONV} \quad (5)$$

where P_{BAT_0} is the state of charge of the battery bank at the previous time step, α_2 is the hourly self-discharge rate (0.0001), P_{REN} is the available renewable power, P_{ELE} is the power consumption of the electrolyzer, and η_{ELE} is the electrolyzer's efficiency. On the other hand, in order to check that the capacity of the battery bank is not below the minimum state of charge, the virtual state of discharge (VSOD) must be calculated as shown in Equation (6).

$$VSOD = P_{BAT_0}(1 - \alpha_2) - \left(\frac{P_{NEEDED}}{\eta_{BAT} \cdot \eta_{CONV}} \right) \quad (6)$$

where P_{NEEDED} is the power needed to meet the energy demand of the electrolyzer, which is explained in detail in Section 3.4.2.

3.2.4. Electrolyzer and Hydrogen Storage Tank

An electrolyzer is a device whose function consists in dissociating hydrogen and oxygen from water. An electrolyte separates an anode and a cathode. When the electric current passes through the electrolyte, a chemical reaction takes place. In the present study, a proton-conducting exchange membrane electrolyzer (PEM) is considered. The hydrogen produced is stored in the hydrogen tank. The energy consumed by the electrolyzer (P_{ELE}) during the process is expressed by Equation (7).

$$P_{ELE} = (P_{REN} + P_{BAT} \cdot \eta_{BAT} \cdot \eta_{CONV}) \eta_{ELE} \quad (7)$$

where P_{BAT} is the current state of charge of the battery bank. The mass of hydrogen obtained during the process depends on the energy available in the electrolyzer. Furthermore, the production of hydrogen at time $H_2(t)$ is limited by the capacity of the electrolyzer, as explained in Equation (8).

$$H_2(t) = \frac{P_{ELE}}{ECK} \leq HT_{max} \quad (8)$$

where ECK is the consumption energy per kilogram of hydrogen produced (55 kWh/kg [47]) and HT_{max} is the maximum capacity of the hydrogen storage tank.

3.3. Problem Formulation

The problem formulation takes into account economic, production, efficiency, and reliability indicators. The main objective of this study consists of proposing the optimal combination of system devices to minimize the energy cost (EC) and the wasted energy (WE), while maximizing the energy delivered to the grid (P_{SOLD}). The daily demand of hydrogen must be met, which is guaranteed by a penalty. The objective function of the problem is shown in Equation (9).

$$\min_x(OF) = \beta_1 EC - \beta_2 P_{SOLD} + \beta_3 WE + Penalty \quad (9)$$

where β_i are the normalization factors used to balance the objectives of the objective function. They must guarantee the normalization of the objectives to values between 0 and 1. The values that guarantee such a condition are 1 , 10^{-7} , and 10^{-6} to β_1 , β_2 , and β_3 , respectively. Furthermore, X depicts the decision variables of the problem, which are shown in Equation (10).

$$X = (PV_N WT_N P_{ELE} NH) \tag{10}$$

where PV_N is the number of solar photovoltaic modules, WT_N is the number of wind turbines, P_{ELE} is the dimension of the electrolyzer (kWh), and NH is the number of hours of autonomy of the battery bank, as explained above.

The economic indicator is represented by the energy cost. In order to compute this indicator, the total net present cost ($TNPC$) must be calculated as shown in Equation (11) [16]. The $TNPC$ depicts the main investment and operating expenditures over the project lifetime.

$$TNPC = \frac{ACS}{CRF} \tag{11}$$

where ACS is the annualized cost of the system (€/year) and CRF denotes the capital recovery factor, which is computed using Equation (12).

$$CRF = \frac{i_r(1 + i_r)^n}{(1 + i_r)^n - 1} \tag{12}$$

where i_r is the annual rate of interest, and n is the system’s lifetime (25 years). Furthermore, i_r is computed using Equation (13), which considers the interest rate (int) (6%) and the inflation rate (4%).

$$i_r = \frac{int - inflation\ rate}{1 + inflation\ rate} \tag{13}$$

Regarding ACS , it is composed using the annualized cost of the system’s devices (ACD_i), as shown in Equation (14).

$$ACS = ACD_{PV} + ACD_{INV} + ACD_{WT} + ACD_{BAT} + ACD_{CONV} + ACD_{ELE} + ACD_{HT} \tag{14}$$

Furthermore, the annualized cost of each device is composed of its annual capital cost (ACC), annual replacement cost (ARC), and annual operation and maintenance cost ($AOMC$) (see Equation (15)).

$$ACD_i = ACC_i + ARC_i + AOMC_i \tag{15}$$

Therefore, it is necessary to compute these terms in relation to the number of photovoltaic modules; the number of wind turbines; and the dimensions of the inverter, the battery bank, the converter, the electrolyzer, and the hydrogen tank. For each device i , its lifetime must be used to compute both its ACC_i (see Equation (16)) and its ARC_i (see Equation (17) [48]).

$$ACC_i = CRF_i \times CC_i \tag{16}$$

$$ARC_i = RC_i \times \frac{(LT_{sys} - LT_i)}{LT_i} \tag{17}$$

where CC_i is the capital cost of the device i , RC_i is the replacement cost of the device i , LT_{sys} is the lifetime of the system, and LT_i is the lifetime of the device i . Finally, the energy cost EC can be computed using Equation (18).

$$EC(\text{€}/kWh) = \frac{TNPC(\text{€}) \times CRF}{\sum_1^{8760} P_{REN}(kWh)} \tag{18}$$

The production indicator is depicted by the energy delivered to the grid (P_{SOLD}). When the renewable energy produced exceeds the maximum capacity of both the electrolyzer and the battery bank, a portion of this energy can be delivered to the grid, which is an objective to maximize. However, the company that manages the energy market plans on a day-to-day basis how much renewable energy it will receive from the producers. Therefore, not all excess energy will be absorbed by the grid. Excess energy that is not absorbed is wasted energy (WE). This is the efficiency indicator considered in the objective function, which is an objective to minimize (see Equation (19)).

$$WE = \sum_1^{8760} \left(P_{REN} - \frac{P_{ELE}}{\eta_{ELE}} - P_{SOLD} \right) \tag{19}$$

Finally, the reliability indicator is included in the objective function as a penalty function. Its function consists of penalizing solutions where the daily hydrogen demand is not met. Such a circumstance is controlled by computing the daily loss of hydrogen production probability ($LHPP$), as explained in Equation (20).

$$LHPP = \sum_1^{365} \left(1 - \left(\frac{D_{H_2} - U_{H_2}}{D_{H_2}} \right) \right) \tag{20}$$

where D_{H_2} is the daily hydrogen demand and U_{H_2} is the daily unmet hydrogen demand. The problem is subject to some limit values and constraints, as shown in Equation (21):

$$\begin{aligned} PV_{N_{min}} &\leq PV_N \leq PV_{N_{max}} \\ WT_{N_{min}} &\leq WT_N \leq WT_{N_{max}} \\ P_{ELE_{min}} &\leq P_{ELE} \leq P_{ELE_{max}} \\ NH_{min} &\leq NH \leq NH_{max} \\ LHPP &= 0 \end{aligned} \tag{21}$$

3.4. The Optimization Process

Next, the simulation process and the dispatch strategy are shown in detail. Moreover, the scatter search implementation is exposed.

3.4.1. The Simulation Process

The simulation process is depicted in Algorithm 1.

It can be seen that the algorithm starts by reading the configuration file, in which the limit values of the decision variables and the stopping criterion are set. Next, the ambient temperature, wind speed, and solar irradiance are extracted from the meteorological data source. Finally, the renewable energy demand is achieved from the energy market.

Once these data are available, the optimization process starts. For the daily demand of hydrogen and the configuration of the optimization method a population must be generated. Each individual in the population must be evaluated. Therefore, once the energy generated from renewable sources has been computed, the dispatch strategy is simulated, the objective function is evaluated, and the population is updated. The optimizer evolves the population until reaching the stopping criterion.

Algorithm 1 Algorithm of the simulation process.

```

1: parameters ← config.txt
2:  $T_A(t), v_h(t), I(t)$  ← meteo()
3:  $D_{EOLIC}, D_{SOLAR}$  ← market()
4: for <Hydrogen demands> do
5:   for <method conditions> do
6:     Generate Population
7:     Compute Renewable Power
8:     Simulate Dispatch Strategy
9:     Evaluate Objective Function
10:    Update population
11:    while <Stopping criterion> do
12:      Evolve Population
13:      Compute Renewable Power
14:      Simulate Dispatch Strategy
15:      Evaluate Objective Function
16:      Update population
17:    end while
18:  end for
19: end for

```

3.4.2. The Dispatch Strategy

The dispatch strategy shown in Figure 3 explains the process of managing energy in the system. Depending on the capacity of the electrolyzer (X_3) and the number of hours of autonomy (X_4), the maximum capacity of the battery bank can be computed (C_{BAT}). The process starts with a state of charge of the battery bank (P_{BAT_0}) of 80%. The daily demand of hydrogen must be met over a time horizon of one year. At the end of every day, the hydrogen tank is emptied.

Every hour, the available renewable energy (P_{REN}) feeds the electrolyzer. The daily hydrogen demand (d_{H_2}) must not be exceeded; therefore, the state of charge of the hydrogen tank (HT) must be monitored. When the available renewable energy (P_{REN}) is less than the energy required by the electrolyzer (X_3), the energy needed is computed (P_{NEEDED}), which must be provided by the battery bank ($FROM_{BAT}$). The state of discharge of the battery bank ($VSOD$) cannot be less than 20% of C_{BAT} . Therefore, energy can be provided from the battery bank to the electrolyzer under this condition. On the other hand, when the available renewable energy exceeds the energy required by the electrolyzer, the battery bank is supplied with energy (TO_{BAT}). The state of charge of the battery bank ($VSOC$) cannot exceed its maximum capacity C_{BAT} .

When the available renewable energy is not needed to feed the electrolyzer and the battery bank, it can be delivered to the grid (P_{EXCESS}). However, the energy market sets hourly limits regarding the purchase of renewable energy. These limits are established in relation to each energy source. Therefore, the energy excess must be computed for both solar (P_{EXCESS_PV}) and wind (P_{EXCESS_WT}) energy. In addition, these hourly limits should be shared by all energy producers. The present study considers that the system cannot supply more than 5% of the hourly limits set by the energy market, (S_{WT}) and (S_{PV}).

The available renewable energy that is not employed for the electrolyzer or the battery bank, or that is not delivered to the grid, is considered wasted energy ($DUMP$). At the end of the day, the unmet demand for hydrogen must be computed, in a process that is repeated every day of the year.

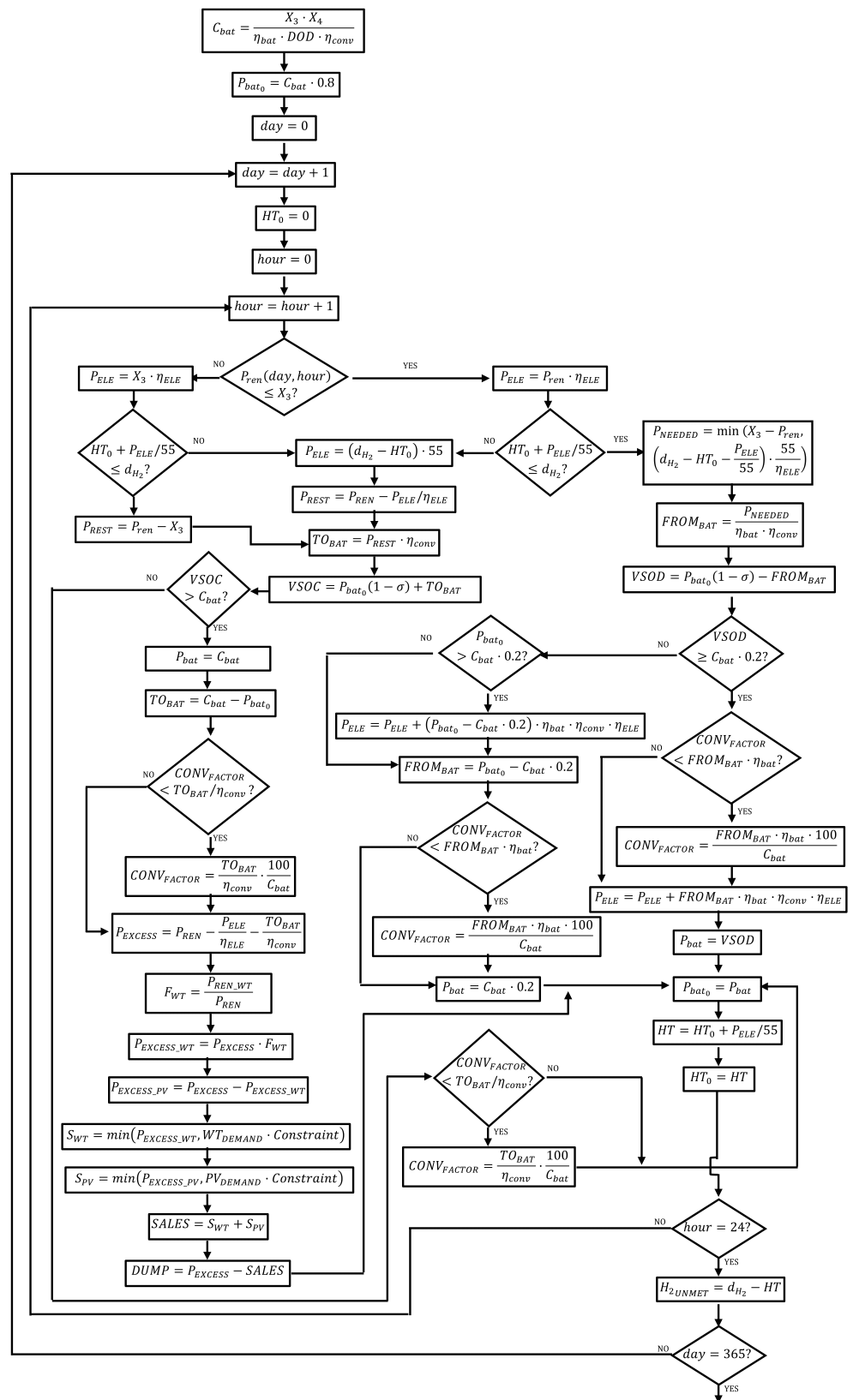


Figure 3. Dispatch strategy.

3.4.3. The Scatter Search Implementation

The scatter search (SS) implementation developed in the present paper is shown by Figure 4. It is explained as follows:

1. A population of individuals (candidate solutions) is randomly created.
2. A reference set of solutions is generated using the best adapted individuals in the population and the most diverse with respect to the best. The best adapted individuals are those with the best value for the objective function. The most diverse individuals are obtained from the remaining individuals through a iterative selection of the most diverse solutions in the population with respect to the solutions already in the reference set.
3. The best individuals in the reference set are combined. The way in which these individuals are combined follows Equation (22). When the value of the objective function of a new individual is better than any of the previous best individuals in the reference set, this new individual replaces the previous best individual.

$$new_{ind} = abs(ind_1 + M \cdot (ind_2 - ind_3)) \tag{22}$$

In this Equation, new_{ind} is the created individual, ind_1 to ind_3 are the individuals combined to create the new individual, and M is a scaling factor between 0.1 and 0.9.

4. The best individuals from the reference set are also combined with the most diverse ones using Equation (22). Now, the most diverse individuals are selected for the reference set. When a new individual is more diverse than that of any of the previous diverse individuals in the reference set, this new individual replaces the previous best individual.
5. These two steps are repeated until the stopping criterion is reached.

Next, the procedure is illustrated using an example. In this case, the aim is to generate a reference set of 5 individuals (the 3 best adapted and the 2 most diverse regarding the previous individuals). A population of 8 individuals (ind. 1 to ind. 8), which is shown in Table 1, is randomly generated. In the example, each individual has 4 characteristics (ch. 1 to ch. 4) that take integer values between 1 and 10. The value of the objective function (OF) is shown in column 6 of Table 1. In the example, it consists of the sum of the characteristics of each individual. Next, the population is ordered according to the value of the objective function, as shown in Table 2. Therefore, the first three individuals in Table 2 are the best adapted, so they are selected for the reference set (individuals 6, 2, and 1).

Table 1. Population of the example.

Individual	Ch. 1	Ch. 2	Ch. 3	Ch. 4	OF
ind. 1	4	4	4	9	21
ind. 2	7	5	6	9	27
ind. 3	6	5	2	1	14
ind. 4	3	7	2	0	12
ind. 5	1	2	8	2	13
ind. 6	1	9	10	9	29
ind. 7	2	3	3	1	9
ind. 8	3	7	5	4	19

Table 2. Ordered population of the example.

Individual	Ch. 1	Ch. 2	Ch. 3	Ch. 4	OF
ind. 6	1	9	10	9	29
ind. 2	7	5	6	9	27
ind. 1	4	4	4	9	21
ind. 8	3	7	5	4	19
ind. 3	6	5	2	1	14
ind. 5	1	2	8	2	13
ind. 4	3	7	2	0	12
ind. 7	2	3	3	1	9

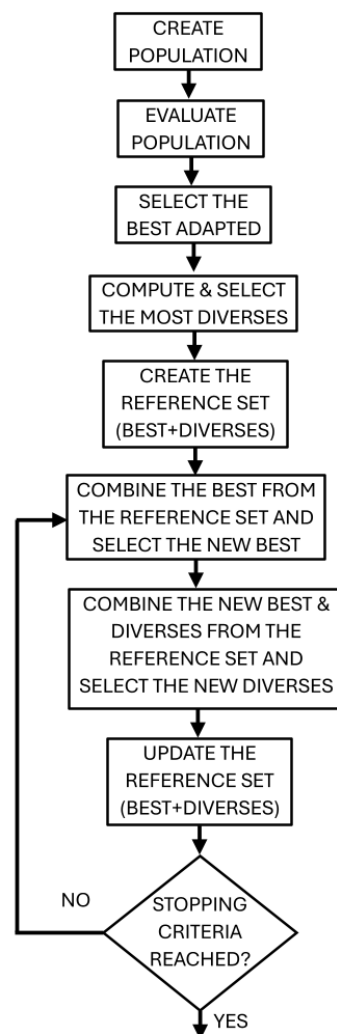


Figure 4. Flow chart of the scatter search implementation.

In order to select the most diverse individuals, each best individual is subtracted as an absolute value with respect to the individuals not selected. As an example, the subtraction of the best individual (ind. 6) and the first from the remainder (ind. 8) gives a value of $|1 - 3| + |9 - 7| + |10 - 5| + |9 - 4| = 14$. Once all subtractions have been computed, Table 3 is generated. Each column relates to each best individual (individuals 6, 2, and 1), and each row relates to each subtraction in absolute value regarding the individual indicated. Next, the minimum value for each row in Table 3 is chosen, and finally, the maximum value of the minimum values previously identified (marked in bold) is the most diverse individual. In the example, the most diverse individual is the individual identified

as ind. 5. The procedure of identifying the most diverse individuals is repeated using the best and most diverse individuals previously identified. The result is shown in Table 4, where the 3 best individuals and the 2 most diverse individuals are displayed. These are the reference set.

Table 3. Distance between the best and the remaining individuals.

Individuals	Ind. 6	Ind. 2	Ind. 1
ind. 8	14	12	10
ind. 3	25	13	13
ind. 5	16	18	16
ind. 4	21	19	15
ind. 7	22	18	12

Table 4. Reference set: the best adapted and most diverse individuals.

Individuals	Ch. 1	Ch. 2	Ch. 3	Ch. 4
Best1—ind. 6	1	9	10	9
Best2—ind. 2	7	5	6	9
Best3—ind. 1	4	4	4	9
Diverse1—ind. 5	1	2	8	2
Diverse2—ind. 3	6	5	2	1

The procedure for updating the reference set continues by combining the best individuals as shown in Equation (22). As an example, the combination of an individual (ind. 6) and the remaining individuals (ind. 2 and ind. 1) provides a new individual, characteristic by characteristic. As an example, the value of the M parameter is set to 0.6. The value of ch. 1 when ind. 2 minus ind. 1 is considered in Equation (22) and calculated as $|1 + 0.6 \times (7 - 4)| = 2.8$. Both alternatives are taken into account; therefore, the value of ch.1 when ind. 1 minus ind. 2 considered in Equation (22) is $|1 + 0.6 \times (4 - 7)| = 0.8$. The set of individuals obtained after these combinations are shown in Table 5. They have been reordered according to their fitness function and selected by the number considered (the first 3 for the example case). All other individuals have been discarded.

Table 5. The result of combining and ordering the best individuals.

Ch. 1	Ch. 2	Ch. 3	Ch. 4	OF
2.8	9.6	11.2	9	32.6
5.2	8	9.6	9	31.8
1	9	10	9	29
7	5	6	9	27
0.8	8.4	8.8	9	27
8.8	2	2.4	9	22.2
0.4	6.4	6.4	9	22.2
4	4	4	9	21
7.6	1.6	1.6	9	19.8

The three best adapted individuals should then be combined with the two most diverse individuals previously identified by following Equation (22). As an example, the combination of the first characteristic of the new best individual and the most diverse individuals from the reference set (ind. 5 and ind. 3) provides a value of $|2.8 + 0.6 \times (1 - 6)| = 5.8$. The individuals generated are shown in Table 6.

Table 6. The result of combining the best and the most diverse individuals.

Ch. 1	Ch. 2	Ch. 3	Ch. 4
5.8	11.4	7.6	8.4
0.2	7.8	14.8	9.6
8.2	9.8	6	8.4
2.2	6.2	13.2	9.6
4	10.8	6.4	8.4
2	7.2	13.6	9.6

After repeating the procedure to select the most diverse individuals, a reference set will be formed again by the three best adapted and the two most diverse individuals. The reference set obtained after the first iteration of the example is shown in Table 7. This is updated iteratively following the above rules.

Table 7. The reference set.

Individual	Ch. 1	Ch. 2	Ch. 3	Ch. 4
Best1	2.8	9.6	11.2	9
Best2	5.2	8	9.6	9
Best3	1	9	10	9
Diverse1	6	5	2	1
Diverse2	1	2	8	2

3.5. Scope of the Experiment

This paper explored differential evolution, a genetic algorithm, the optimal foraging algorithm, and scatter search to achieve the optimal sizing of a hybrid renewable system with hydrogen technologies. The differential evolution, genetic algorithm, and optimal foraging algorithm implementations were taken from PlatEMO [49]. The aim of the experiment was to explore the performance of the methods and compare their performance. These algorithms include certain configuration parameters, as shown in Table 8. The main parameters used to configure these methods are described as follows:

- **Mutation Probability (PrM):** This parameter depicts the probability of the number of genes that will mutate. The value of PrM considered was equivalent to 1/decision variables when differential evolution was used. When the genetic algorithm was employed, two more probabilities were used, one above and the other one below this central value (1.5/decision variables and 0.5/decision variables, respectively).
- **Mutation Distribution (disM):** This parameter is the distribution index of polynomial mutation. After checking that it had little effect on the optimization process, it was set to the typical value of 20. This parameter was used for both the differential evolution and the genetic algorithm.
- **Crossover Probability (PrC):** This is the probability of performing a crossover when the genetic algorithm is used. The crossover operator has an impact on the creation of new individuals. It was set to 1 in this case.
- **Crossover Distribution (disC):** This is the crossover distribution index when the genetic algorithm is used. After checking that it had little effect on the optimization process, this was set to the typical value of 20.
- **Crossover Rate (CR):** This differential evolution operator favors the mixing of genetic information between individuals to create new individuals. Depending on the crossover rate, each gene is crossed (or not). The crossover rate was set at 0.9 (its typical value ranges between 0.1 and 1 [50]) given that a high value tends to speed up convergence [37].
- **Scale Factor (F):** This differential evolution parameter is used to scale the difference vector that is employed by the mutation operator. This operator adds a scaled difference vector from two chosen chromosomes to a third chromosome, in order to alter

the genes of the chromosome. Typical values range from 0.4 to 0.9 [50]. In the present study, values of 0.5, 0.7 and 0.9 were tested.

A parameter exclusively used by the optimal foraging algorithm (λ) is randomly generated in the implementation of the method. This parameter, which takes values between 0 and 1, is used to replace solutions. Regarding the scatter search method, the main parameters considered to generate the reference set are the number of best adapted individuals and the number of most diverse individuals. In scatter search, the reference set is about one order of magnitude smaller than in genetic algorithms [32]. In the present research, with an overall number of 20 individuals, several options were tested, as can be seen in Table 8. Regarding the factor used to create new individuals (M), after testing a range of values between 0.1 and 0.9 (including random generation), the most promising value was 0.6.

Populations of 50, 100, and 150 individuals were tested for the differential evolution, the genetic algorithm, and the optimal foraging algorithm methods. Similar values were considered to generate the initial population for the scatter search method, although only 20 were selected for the reference set. This decision was taken with the idea of starting the simulations from identical conditions. The stopping criterion consisted of 15,000 evaluations of the objective function. However, the number of evaluations needed to reach the best value of the objective function was used to reveal the computational cost. The number of simulations per configuration was thirty-one (for statistical purposes). Three green hydrogen production scenarios were analyzed in order to schedule 100, 200, and 300 kg per day.

Table 8. Set of parameters for the optimization process.

Method	PrC	disC	PrM	disM	CR	F	Best	Diverse	M
DE	-	-	1	20	0.9	0.5 0.7 0.9	-	-	-
GA	1	20	0.5 1.0 1.5	20	-	-	-	-	-
OFA	-	-	-	-	-	-	-	-	-
SS	-	-	-	-	-	-	5 10 15	15 10 5	0.6

Data Background

The area considered for the study is located in Arinaga, on the island of Gran Canaria, Spain. As mentioned above, meteorological data were extracted from Copernicus for all hours of the year 2022. Figure 5 shows the data regarding the ambient temperature (Figure 5a) and solar irradiance (Figure 5b) in the area. Figure 6 shows the wind speed at the height of interest.

As explained above, the grid connection of the hybrid renewable system with hydrogen technologies allowed excess energy to be supplied according to energy market constraints. The energy market sets hourly solar and wind power purchase limits. In order to create a demand profile to use in the study, such limits were observed on various days over several weeks. These values were extrapolated and a profile was generated for all hours of the year. The demand profiles regarding solar and wind purchase limits are shown in Figure 7a,b, respectively.

Parameters regarding the devices considered in the design are shown in Table 9.

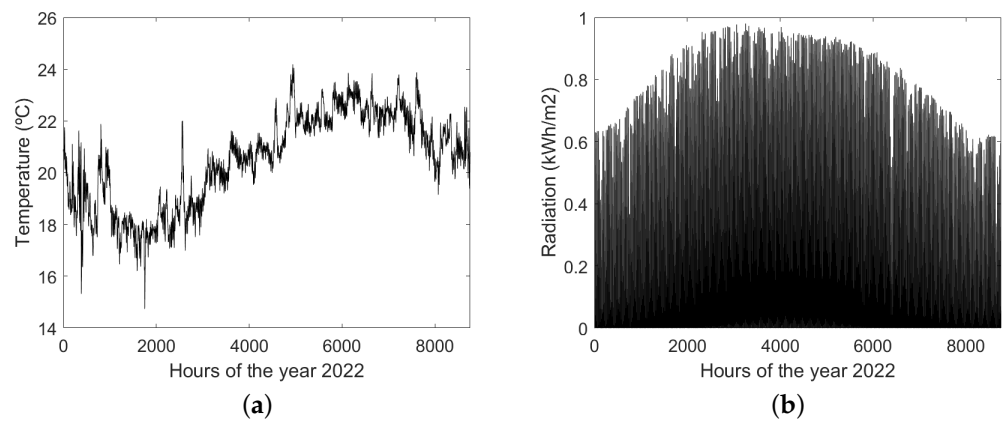


Figure 5. Meteorological data used to compute renewable solar energy. (a) Ambient temperature; (b) solar irradiance.

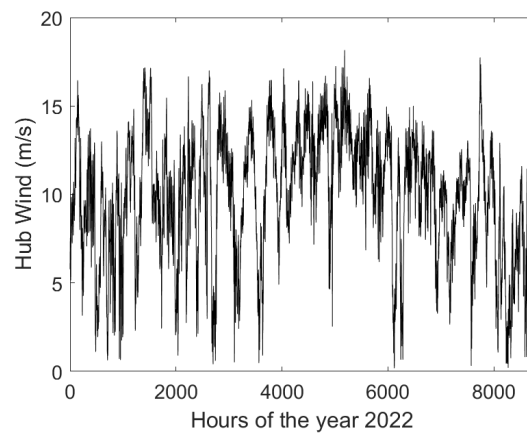


Figure 6. Wind speed at the height of interest.

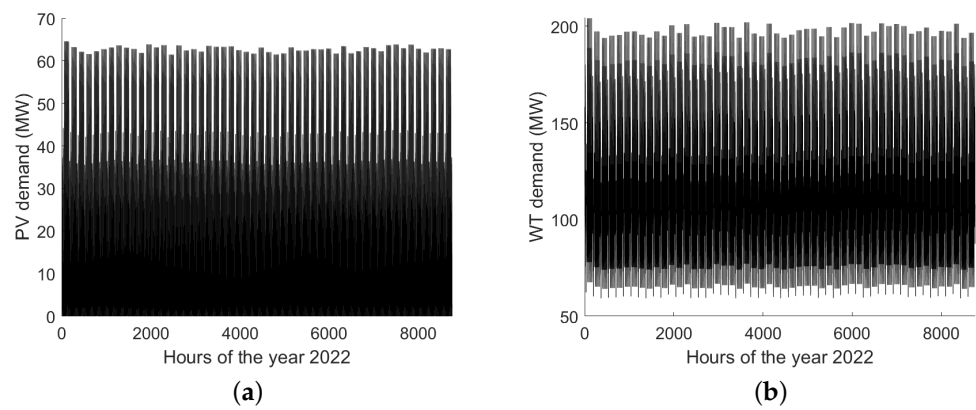


Figure 7. Hourly energy demand. (a) Hourly solar energy demand; (b) hourly wind energy demand.

Table 9. List of system parameters.

Parameter	Value
$PV_{N_{min}}$: Minimum number of solar photovoltaic modules	0
$PV_{N_{max}}$: Maximum number of solar photovoltaic modules	15,000
$WT_{N_{min}}$: Minimum number of wind turbines	0
$WT_{N_{max}}$: Maximum number of wind turbines	15
$P_{ELE_{min}}$: Minimum power of the electrolyzer (kWh)	200
$P_{ELE_{max}}$: Maximum power of the electrolyzer (kWh)	3000
NH_{min} : Minimum autonomy of the battery bank (h)	1
NH_{max} : Maximum autonomy of the battery bank (h)	2
CC_{PV} : Solar module capital cost (€/module)	$2.5 \times P_{R,PV}$
CC_{INV} : Inverter capital cost (€/kW)	800
CC_{WT} : Wind turbine capital cost (€/unit)	120,000
CC_{BAT} : Battery capital cost (€/kW)	1000
CC_{CONV} : Converter capital cost (€/kW)	800
CC_{ELE} : Electrolyzer capital cost (€/kW)	2000
CC_{HT} : Hydrogen tank capital cost (€/kW)	1300
RC_{PV} : Solar module replacement cost (€/module)	$2.5 \times P_{R,PV}$
RC_{INV} : Inverter replacement cost (€/kW)	750
RC_{WT} : Wind turbine replacement cost (€/unit)	120,000
RC_{BAT} : Battery replacement cost (€/kW)	1000
RC_{CONV} : Converter replacement cost (€/kW)	750
RC_{ELE} : Electrolyzer replacement cost (€/kW)	1500
RC_{HT} : Hydrogen tank replacement cost (€/kW)	1200
$AOMC_{PV}$: Solar module annual operation and maintenance cost (€/module)	$0.02 \times CC_{PV}$
$AOMC_{INV}$: Inverter annual operation and maintenance cost (€/kW year)	8
$AOMC_{WT}$: Wind turbine annual operation and maintenance cost (€/unit)	500
$AOMC_{BAT}$: Battery annual operation and maintenance cost (€/kW year)	5
$AOMC_{CONV}$: Converter annual operation and maintenance cost (€/kW)	8
$AOMC_{ELE}$: Electrolyzer annual operation and maintenance cost (€/kW)	25
$AOMC_{HT}$: Hydrogen tank annual operation and maintenance cost (€/kW)	15
LT_{PV} : Solar module lifetime (year)	25
LT_{INV} : Inverter lifetime (year)	15
LT_{WT} : Wind turbine lifetime (year)	20
LT_{BAT} : Battery lifetime (year)	5
LT_{CONV} : Converter lifetime (year)	15
LT_{ELE} : Electrolyzer lifetime (year)	20
LT_{HT} : Hydrogen tank lifetime (year)	20

4. Results of the Optimization

The results obtained are shown below. First, the results obtained by applying the differential evolution method are shown. Second, the results from the genetic algorithm are displayed. Third, the results from the optimal foraging algorithm are given. Fourth, the results obtained by applying the proposed scatter search method are shown. Finally, a comparative study of scatter search with the other three methods is developed and a discussion is provided.

4.1. Differential Evolution

Figure 8a–c show box plots of the experiments in which the differential evolution method was used for the optimal sizing of a hybrid renewable energy system for green hydrogen production. These figures refer to the scheduled production of 100, 200, and 300 kg of green hydrogen per day, respectively. For each scenario, nine cases can be observed. They are described in the first five columns of Table 10, detailing the case identification, the green hydrogen demand satisfied per day, and the method parameters. Each box plot summarizes the statistical results of running 31 simulations for each simulated case.

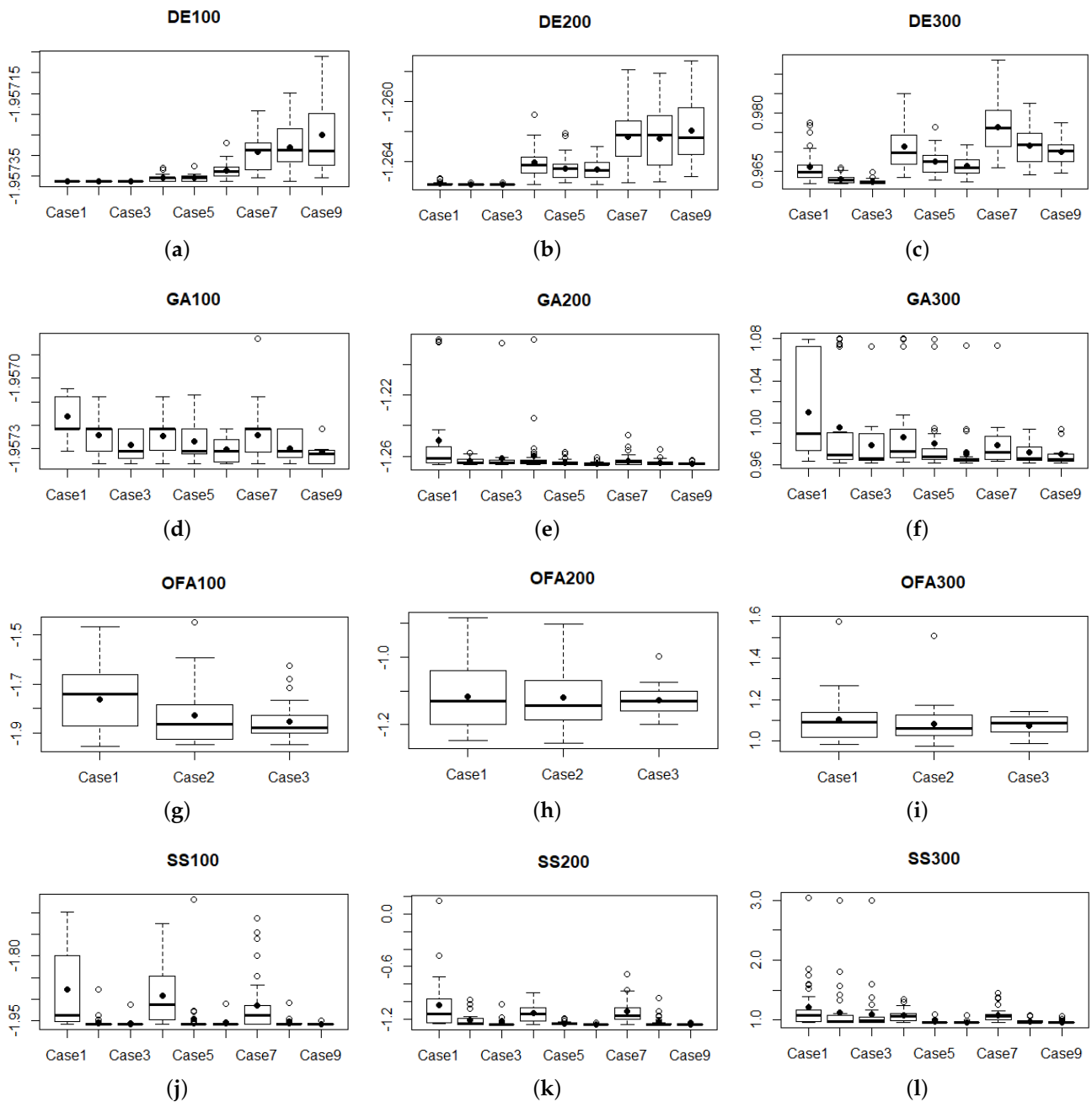


Figure 8. Box plot simulations. (a) Box plot to produce 100 kg/day (DE); (b) box plot to produce 200 kg/day (DE); (c) box plot to produce 300 kg/day (DE); (d) box plot to produce 100 kg/day (GA); (e) box plot to produce 200 kg/day (GA); (f) box plot to produce 300 kg/day (GA); (g) box plot to produce 100 kg/day (OFA); (h) box plot to produce 200 kg/day (OFA); (i) box plot to produce 300 kg/day (OFA); (j) box plot to produce 100 kg/day (SS); (k) box plot to produce 200 kg/day (SS); (l) box plot to produce 300 kg/day (SS).

Graphically, it can be seen that Cases 1 to 3 performed better than Cases 4 to 9 in all scenarios. However, this needs to be confirmed by hypothesis testing. Columns 6 to 10 of Table 10 show the summary statistics for each test case associated with the results obtained with each configuration. From left to right, the minimum, median, pseudo-median, and mean values for the objective function and the *p*-value obtained after using a Saphiro–Wilk test [51] can be seen. The Saphiro–Wilk test is a test of normality which tests whether a sample is from a normally distributed population (the null hypothesis). When

the p -value obtained is less than 0.05, the null hypothesis is rejected and the non-normality of the sample is assumed. In contrast, when the p -value obtained is greater than or equal to 0.05, the null hypothesis is accepted and the normality of the sample is assumed. It can be seen that the configurations DE100C1 to DE100C3 present identical values; that is, in all 31 simulations, the same value for the minimum of the objective function was obtained, the configurations DE100C8, DE200C6 to DE200C9 and DE300C5 to DE300C9 were normally distributed, and the rest were not. Hereafter, for simplicity of notation, for each of the scenarios (production of green hydrogen in quantities of 100, 200, and 300 kg), the configurations using differential evolution are denoted as DE1 to DE9.

Table 10. Differential evolution statistics and Shapiro–Wilk test results.

Case ID	H2 Demand	Population	CR	F	Minimum	Median	Pseudo-Median	Mean	S-W Test
DE100C1	100	50	0.9	0.5	−1.95736	−1.95736	-	−1.95736	Identical values
DE100C2	100	50	0.9	0.7	−1.95736	−1.95736	-	−1.95736	Identical values
DE100C3	100	50	0.9	0.9	−1.95736	−1.95736	-	−1.95736	Identical values
DE100C4	100	100	0.9	0.5	−1.95736	−1.95735	−1.95736	−1.95736	0.00015
DE100C5	100	100	0.9	0.7	−1.95736	−1.95735	−1.95736	−1.95736	0.00010
DE100C6	100	100	0.9	0.9	−1.95736	−1.95734	−1.95736	−1.95734	0.01421
DE100C7	100	150	0.9	0.5	−1.95735	−1.95729	−1.95727	−1.95729	0.0338
DE100C8	100	150	0.9	0.7	−1.95736	−1.95729	-	−1.95728	0.3384
DE100C9	100	150	0.9	0.9	−1.95735	−1.95729	−1.95726	−1.95725	0.00059
DE200C1	200	50	0.9	0.5	−1.26552	−1.26552	−1.26552	−1.26547	6.9×10^{-9}
DE200C2	200	50	0.9	0.7	−1.26552	−1.26552	−1.26552	−1.26551	2.5×10^{-11}
DE200C3	200	50	0.9	0.9	−1.26552	−1.26552	−1.26552	−1.26551	2.5×10^{-11}
DE200C4	200	100	0.9	0.5	−1.26552	−1.26423	−1.26416	−1.26407	0.00954
DE200C5	200	100	0.9	0.7	−1.26541	−1.26445	−1.26451	−1.26444	0.00254
DE200C6	200	100	0.9	0.9	−1.26552	−1.26461	-	−1.26454	0.2869
DE200C7	200	150	0.9	0.5	−1.26541	−1.26224	-	−1.26235	0.381
DE200C8	200	150	0.9	0.7	−1.26537	−1.26225	-	−1.26248	0.06822
DE200C9	200	150	0.9	0.9	−1.26498	−1.26241	-	−1.26197	0.07769
DE300C1	300	50	0.9	0.5	0.961812	0.964822	0.96505	0.96612	6.4×10^{-5}
DE300C2	300	50	0.9	0.7	0.961812	0.962799	0.96281	0.96299	0.00186
DE300C3	300	50	0.9	0.9	0.961812	0.962135	0.96211	0.96224	4.6×10^{-7}
DE300C4	300	100	0.9	0.5	0.963468	0.969837	0.97063	0.97140	0.00481
DE300C5	300	100	0.9	0.7	0.962624	0.967444	-	0.96747	0.1693
DE300C6	300	100	0.9	0.9	0.962291	0.965811	-	0.96636	0.2897
DE300C7	300	150	0.9	0.5	0.965843	0.976158	-	0.97622	0.4135
DE300C8	300	150	0.9	0.7	0.963978	0.971676	-	0.97154	0.4501
DE300C9	300	150	0.9	0.9	0.964517	0.970076	-	0.96995	0.4763

Since most of the samples were not normally distributed, a Kruskal–Wallis rank sum test [52] was performed using the *kruskal.test()* function of the *R package stats* [53]. This test allowed determining whether there were significant differences between configurations. For each scenario, the results obtained with differential evolution (DE1 to DE9) were compared. In all three scenarios, p -values of less than 0.05 were obtained. Therefore, significant differences were found between at least one pair of configurations for all green hydrogen production scenarios. Then, a multiple comparison test after Kruskal–Wallis [54] between samples was performed using the *kruskalmc()* function of the *R package pgirmess* [55], to identify which configurations were different with pairwise comparisons adjusted appropriately for multiple comparisons. The upper triangular part of Table 11 shows the results of the multiple comparison test for the configurations using the differential evolution method. In each cell, three letters can be seen that vary between T (true) and F (false). These refer to the green hydrogen demand scenarios of 100, 200, and 300 kg per day, respectively. It can be seen that the multiple comparison test provided nonsignificant differences among the performances of the configurations DE1 and DE2 in all scenarios (FFF). The same

circumstance can be observed for the configurations DE2 and DE3. However, significant differences were observed between configurations DE1 and DE3 in the third scenario (FFT) (demand of 300 kg of green hydrogen per day).

Table 11. Multiple pairwise comparisons (DE).

			DE2	DE3	DE4	DE5	DE6	DE7	DE8	DE9	
DE2	=↑↑		FFF	FFT	FTT	FTF	TTF	TTT	TTT	TTT	DE1
DE3	=↑↑	==↑		FFF	FTT	FTT	TTT	TTT	TTT	TTT	DE2
DE4	↓↓↓	↓↓↓	↓↓↓		FTT	FTT	TTT	TTT	TTT	TTT	DE3
DE5	↓↓↓	↓↓↓	↓↓↓	==↑		FFF	FFF	TFF	TFF	TFF	DE4
DE6	↓↓=	↓↓↓	↓↓↓	↓=↑	↓==		FFF	TFT	TFF	TTF	DE5
DE7	↓↓↓	↓↓↓	↓↓↓	↓↓↓	↓↓↓	↓↓↓		FTT	FFT	TTF	DE6
DE8	↓↓↓	↓↓↓	↓↓↓	↓↓=	↓↓↓	↓↓↓	==↑		FFF	FFF	DE7
DE9	↓↓↓	↓↓↓	↓↓↓	↓↓=	↓↓↓	↓↓↓	==↑	===		FFF	DE8
	DE1	DE2	DE3	DE4	DE5	DE6	DE7	DE8			

Once significant differences had been verified regarding the multiple comparisons test, the appropriate test for pairwise comparisons was used. When samples came from a normally distributed population, a Student test was used. Conversely, when samples did not come from a normally distributed population, the Wilkonson rank sum test (equivalent to the Mann–Whitney test) was used. The lower triangular part of Table 11 shows the result of pairwise comparisons (columns vs. rows) between the configurations of the differential evolution (DE) method. The Student test or the Mann–Whitney test were appropriately used. In each cell, three symbols can be seen. They refer to demands of 100, 200, and 300 kg of hydrogen per day, respectively. The symbol = means that no significant differences were found between the compared samples, the symbol ↑ means that the column sample is shifted to the right of the row sample (i.e., the column sample has higher objective function values than the row sample) and the symbol ↓ indicates that the column sample is shifted to the left of the row sample (i.e., the column sample has lower objective function values than the row sample). As an example, focusing on configurations DE1 and DE2 it can be seen that non-significant differences were found for the scenario of 100 kg of green hydrogen per day. However, significant differences were found for the scenarios of 200 and 300 kg of green hydrogen per day, in which the configuration DE1 obtained higher objective function values than the configuration DE2. Nevertheless, the multiple comparisons test showed that non-significant differences were found between the performance of the DE1 and DE2 configurations in the three scenarios. A similar behavior can be observed when comparing the DE1 and DE3 configurations. Regarding the configurations DE2 and DE3 it can be seen that DE2 provided equal performance in the scenarios of 100 and 200 kg, and was lower in the scenario of 300 kg. The configurations DE1 DE2 and DE3 matched or outperformed the other configurations in all scenarios, and the configuration DE2 provided a slight advantage over configurations DE1 and DE2.

4.2. Genetic Algorithm

Figure 8d–f show box plots of experiments in which the genetic algorithm was used for the optimal sizing of a hybrid renewable energy system for green hydrogen production. These figures refer to the scheduled production of 100, 200, and 300 kg of green hydrogen per day, respectively. For each scenario, nine cases can be observed. They are described in the first five columns of Table 12, detailing the case identification, the green hydrogen demand satisfied per day, and the parameters of the method. Each box plot summarizes the statistical result of running 31 simulations for each simulated case.

Graphically, it can be seen that Cases 6 and 9 performed better than the others in all scenarios. However, this needs to be confirmed by hypothesis testing. Columns 6 to 10 of Table 12 show the summary statistics for each test case associated with the results obtained with each configuration. From left to right, the minimum, median, pseudo-median, and

mean for the objective function value and the *p*-value obtained after using the Shapiro–Wilk test can be seen. It can be seen that all configurations were not normally distributed. For simplicity of notation, for each of the scenarios (production of green hydrogen in quantities of 100, 200, and 300 kg), configurations using the genetic algorithm are denoted as GA1 to GA9.

Table 12. Genetic algorithm statistics and Shapiro–Wilk test results.

Case ID	H2 Demand	Population	PrC	disC	Minimum	Median	Pseudo-Median	Mean	S-W Test
GA100C1	100	50	0.5	20	−1.95731	−1.95721	−1.95718	−1.95716	3.5×10^{-5}
GA100C2	100	50	1.0	20	−1.95736	−1.95721	−1.95723	−1.95724	0.00010
GA100C3	100	50	1.5	20	−1.95736	−1.95731	−1.95729	−1.95728	3.1×10^{-5}
GA100C4	100	100	0.5	20	−1.95736	−1.95721	−1.95723	−1.95725	0.00026
GA100C5	100	100	1.0	20	−1.95736	−1.95731	−1.95727	−1.95727	0.00037
GA100C6	100	100	1.5	20	−1.95736	−1.95731	−1.95729	−1.95730	4.1×10^{-5}
GA100C7	100	150	0.5	20	−1.95736	−1.95721	−1.95723	−1.95724	5.7×10^{-5}
GA100C8	100	150	1.0	20	−1.95736	−1.95731	−1.95729	−1.95730	3.2×10^{-5}
GA100C9	100	150	1.5	20	−1.95736	−1.95732	−1.95729	−1.95731	1.6×10^{-5}
GA200C1	200	50	0.5	20	−1.26537	−1.26140	−1.25875	−1.24990	2.9×10^{-8}
GA200C2	200	50	1.0	20	−1.26552	−1.26423	−1.26366	−1.26342	0.00117
GA200C3	200	50	1.5	20	−1.26552	−1.26426	−1.26407	−1.26152	1.7×10^{-11}
GA200C4	200	100	0.5	20	−1.26552	−1.26402	−1.26393	−1.25999	1.5×10^{-10}
GA200C5	200	100	1.0	20	−1.26552	−1.26477	−1.26467	−1.26412	1.2×10^{-6}
GA200C6	200	100	1.5	20	−1.26552	−1.26537	−1.26507	−1.26482	4.0×10^{-7}
GA200C7	200	150	0.5	20	−1.26552	−1.26402	−1.26393	−1.26292	1.7×10^{-7}
GA200C8	200	150	1.0	20	−1.26552	−1.26504	−1.26470	−1.26427	1.2×10^{-7}
GA200C9	200	150	1.5	20	−1.26552	−1.26504	−1.26508	−1.26492	5.8×10^{-6}
GA300C1	300	50	0.5	20	0.963296	0.989643	1.01927	1.00986	9.2×10^{-6}
GA300C2	300	50	1.0	20	0.961967	0.969716	0.97913	0.99584	4.5×10^{-7}
GA300C3	300	50	1.5	20	0.961812	0.966092	0.96968	0.97844	3.2×10^{-8}
GA300C4	300	100	0.5	20	0.962799	0.972806	0.97908	0.98611	4.3×10^{-7}
GA300C5	300	100	1.0	20	0.961967	0.967619	0.96947	0.98069	9.3×10^{-9}
GA300C6	300	100	1.5	20	0.961967	0.964723	0.96479	0.97012	2.1×10^{-10}
GA300C7	300	150	0.5	20	0.963296	0.971911	0.97499	0.97839	1.0×10^{-7}
GA300C8	300	150	1.0	20	0.961967	0.966092	0.96748	0.97191	1.3×10^{-6}
GA300C9	300	150	1.5	20	0.961812	0.964784	0.96698	0.97015	1.0×10^{-6}

Since the samples were not normally distributed, a Kruskal–Wallis rank sum test was performed. For each scenario, the results obtained with the genetic algorithm (GA1 to GA9) were compared. In all scenarios, *p*-values of less than 0.05 were obtained. Therefore, significant differences were found between at least one pair of configurations for each green hydrogen production scenario. Then, after Kruskal–Wallis, a multiple comparison test between samples was performed to identify which configurations were different, with pairwise comparisons adjusted appropriately for multiple comparisons. The upper triangular part of Table 13 shows the results of the multiple comparison test for the configurations employing the genetic algorithm. Again, in each cell, three letters can be seen that vary between T (true) and F (false). These refer to the green hydrogen demand scenarios of 100, 200, and 300 kg per day, respectively. It can be seen that the multiple comparisons test provided non-significant differences among the performances of the configurations GA3, GA5, GA6, GA8, and GA9 in all scenarios.

Table 13. Multiple and pairwise comparisons (GA).

			GA2	GA3	GA4	GA5	GA6	GA7	GA8	GA9	
GA2	↑↑↑		FFF	TTT	TFF	TTF	TTT	TTF	TTT	TTT	GA1
GA3	↑↑↑	↑===		FFF	FFF	FFF	FTT	FFF	FFF	FFF	GA2
GA4	↑↑↑	====	====		FFF	FFF	FFF	FFF	FFF	FFF	GA3
GA5	↑↑↑	====	====	⇒↑=		FFF	FTT	FFF	FFF	FFF	GA4
GA6	↑↑↑	↑↑↑	⇒↑=	↑↑↑	⇒↑=		FFF	FFF	FFF	FFF	GA5
GA7	↑↑↑	====	====	====	====	↓↓↓		FFT	FFF	FFF	GA6
GA8	↑↑↑	↑↑=	====	↑↑↑	====	====	↑=↑		FFF	FFF	GA7
GA9	↑↑↑	↑↑↑	⇒↑=	↑↑↑	⇒↑=	====	↑=↑	====		FFF	GA8
	GA1	GA2	GA3	GA4	GA5	GA6	GA7	GA8			

Once significant differences were found from the multiple comparisons test, the Mann-Whitney test was performed for pairwise comparisons. The lower triangular part of Table 13 shows the result of pairwise comparisons (columns vs. rows) between the configurations of the genetic algorithm (GA). Again, in each cell, three symbols can be seen. They refer to demands of 100, 200, and 300 kg of green hydrogen per day, respectively.

As an example, pairwise comparisons between the GA6 configuration and the others can be seen. In general, the GA6 configuration outperformed configurations GA1 to GA7 in all scenarios, except in the first and third scenarios of the configurations GA3 and GA5 where non-significant differences were obtained. Due to the fact that the problem to be solved was to minimize, configurations GA6, GA8 and GA9 provided a clear advantage.

4.3. Optimal Foraging Algorithm

Figure 8g–i show box plots of experiments in which the optimal foraging algorithm was used for the optimal sizing of a hybrid renewable energy system for green hydrogen production. These figures refer to the scheduled production of 100, 200, and 300 kg of green hydrogen per day, respectively. For each scenario, three cases can be observed. They are described in the first three columns of Table 14, detailing the case identification, the green hydrogen demand satisfied per day, and the population size. Each box plot summarizes the statistical result of running 31 simulations for each simulated case.

Graphically, it can be seen that Case 3 performed better than the others in all scenarios. However, this needs to be confirmed by hypothesis testing. Columns 4 to 8 of Table 14 show the summary statistics for each test case associated with the results obtained with each configuration. From left to right, the minimum, median, pseudo-median, and mean for the objective function value and the *p*-value obtained after using the Shapiro–Wilk test can be seen. It can be seen that there are both normally and not normally distributed configurations. For simplicity of notation, for each of the scenarios (production of green hydrogen in quantities of 100, 200, and 300 kg), configurations using the optimal foraging algorithm are denoted as OFA1 to OFA3.

Table 14. Optimal foraging algorithm statistics and Shapiro–Wilk test results.

Case ID	H2 Demand	Population	Minimum	Median	Pseudo-Median	Mean	S-W Test
OFA100C1	100	50	−1.95447	−1.74259	-	−1.11557	0.1445
OFA100C2	100	100	−1.94740	−1.86275	−1.84438	−1.12004	0.00078
OFA100C3	100	150	−1.94762	−1.87725	−1.86474	−1.12828	0.00154
OFA200C1	200	50	−1.24826	−1.13037	-	−1.11557	0.07316
OFA200C2	200	100	−1.25485	−1.14289	-	−1.12004	0.2336
OFA200C3	200	150	−1.19837	−1.12888	-	−1.12828	0.1303
OFA300C1	300	50	0.983423	1.092488	1.08905	1.10481	2.9×10^{-5}
OFA300C2	300	100	0.976409	1.062644	1.07206	1.08354	3.4×10^{-6}
OFA300C3	300	150	0.987381	1.08935	1.07811	1.07676	0.05847

Next, a Kruskal–Wallis rank sum test was performed. For each scenario, the results obtained with the optimal foraging algorithm (OFA1 to OFA3) were compared. Only in the first scenario was the *p*-value less than 0.05 and significant differences were found between at least one pair of configurations for this green hydrogen production scenario. The upper triangular part of Table 15 shows the results of the multiple comparisons test after Kruskal–Wallis for the configurations employing the optimal foraging algorithm. Again, in each cell, three letters can be seen that vary between T (true) and F (false). These refer to the green hydrogen demand scenarios of 100, 200, and 300 kg per day, respectively. It can be seen that the multiple comparisons test provided non-significant differences among the performances of, on the one hand, the configurations OFA1 and OFA2, and, on the other hand, the configurations OFA2 and OFA3. However, there was a significant difference in the first scenario when OFA1 and OFA3 were compared.

Table 15. Multiple and pairwise comparisons (OFA).

			OFA2	OFA3	
OFA2	====		FFF	TFF	OFA1
OFA3	↑==	====		FFF	OFA2
	OFA1	OA2			

The lower triangular part of Table 15 shows the results of the Mann–Whitney test of pairwise comparisons (columns vs. rows) between the configurations of the optimal foraging algorithm (OFA). Again, in each cell, three symbols can be seen. They refer to demands of 100, 200, and 300 kg of green hydrogen per day, respectively. It can be seen that the OFA3 configuration outperformed configuration OFA1 only in the first scenario. Non-significant differences were obtained regarding the other configurations.

4.4. Scatter Search

Figure 8j–l show box plots of experiments in which the scatter search method was used for the optimal sizing of a hybrid renewable energy system for green hydrogen production. These figures refer to the scheduled production of 100, 200, and 300 kg of green hydrogen per day, respectively. For each scenario, nine cases can be observed. They are described in the first five columns of Table 16, detailing the case identification, the green hydrogen demand satisfied per day, and the parameters of the method. Each box plot summarizes the statistical results of running 31 simulations for each simulated case.

Graphically, it can be seen that Cases 6 and 9 performed better than the others in all scenarios. However, this needs to be confirmed by hypothesis testing. Columns 6 to 10 of Table 16 show the summary statistics for each test case associated with the results obtained with each configuration. From left to right, the minimum, median, pseudo-median, and mean for the objective function value and the *p*-value obtained after using the Shapiro–Wilk test can be seen. It can be seen that all configurations were not normally distributed. For simplicity of notation, for each of the scenarios (production of green hydrogen in quantities of 100, 200, and 300 kg), configurations using scatter search are denoted as SS1 to SS9.

Table 16. Scatter search statistics and Shapiro–Wilk test results.

Case ID	H2 Demand	Population	Best	Diverse	Minimum	Median	Pseudo-Median	Mean	S-W Test
SS100C1	100	50	5	15	−1.95736	−1.93686	−1.87748	−1.87685	1.9×10^{-5}
SS100C2	100	100	5	15	−1.95736	−1.95735	−1.95724	−1.95288	1.0×10^{-10}
SS100C3	100	150	5	15	−1.95736	−1.95736	−1.95736	−1.95585	5.4×10^{-12}
SS100C4	100	50	10	10	−1.95736	−1.91125	−1.89356	−1.89131	0.0091
SS100C5	100	100	10	10	−1.95736	−1.95736	−1.95728	−1.94571	1.3×10^{-11}
SS100C6	100	150	10	10	−1.95736	−1.95736	−1.95736	−1.95571	7.1×10^{-12}
SS100C7	100	50	15	5	−1.95736	−1.93638	−1.93486	−1.91337	5.5×10^{-7}

Table 16. Cont.

Case ID	H2 Demand	Population	Best	Diverse	Minimum	Median	Pseudo-Median	Mean	S-W Test
SS100C8	100	100	15	5	−1.95736	−1.95736	−1.95690	−1.95454	1.1×10^{-10}
SS100C9	100	150	15	5	−1.95736	−1.95736	−1.95736	−1.95709	7.0×10^{-12}
SS200C1	200	50	0.9	0.5	−1.26008	−1.14601	−1.10363	−1.04129	1.9×10^{-6}
SS200C2	200	50	0.9	0.7	−1.26552	−1.25678	−1.25172	−1.21861	1.5×10^{-7}
SS200C3	200	50	0.9	0.9	−1.26552	−1.26552	−1.26495	−1.24985	4.0×10^{-10}
SS200C4	200	100	0.9	0.5	−1.26552	−1.14450	−1.14120	−1.13520	0.0185
SS200C5	200	100	0.9	0.7	−1.26552	−1.25959	−1.25746	−1.25341	1.3×10^{-6}
SS200C6	200	100	0.9	0.9	−1.26552	−1.26552	−1.26462	−1.26369	2.6×10^{-9}
SS200C7	200	150	0.9	0.5	−1.26451	−1.16851	−1.14522	−1.11779	0.00037
SS200C8	200	150	0.9	0.7	−1.26552	−1.26143	−1.25909	−1.23934	2.3×10^{-9}
SS200C9	200	150	0.9	0.9	−1.26552	−1.26552	−1.26440	−1.26263	3.1×10^{-8}
SS300C1	300	50	0.9	0.5	0.961812	1.073780	1.08554	1.21597	8.2×10^{-8}
SS300C2	300	50	0.9	0.7	0.961812	0.983307	1.02239	1.13211	2.0×10^{-9}
SS300C3	300	50	0.9	0.9	0.961812	0.989372	1.00298	1.09959	3.4×10^{-10}
SS300C4	300	100	0.9	0.5	0.961812	1.062328	1.05640	1.07924	0.00016
SS300C5	300	100	0.9	0.7	0.961812	0.962480	0.96377	0.97239	1.5×10^{-9}
SS300C6	300	100	0.9	0.9	0.961812	0.961812	0.96190	0.96699	1.5×10^{-11}
SS300C7	300	150	0.9	0.5	0.961967	1.059164	1.05078	1.07863	1.9×10^{-5}
SS300C8	300	150	0.9	0.7	0.961812	0.962291	0.96507	0.98152	2.1×10^{-8}
SS300C9	300	150	0.9	0.9	0.961812	0.961812	0.96211	0.96940	3.0×10^{-10}

Since the samples were not normally distributed, a Kruskal–Wallis rank sum test was performed. For each scenario, the results obtained with scatter search (SS1 to SS9) were compared. In all scenarios, *p*-values of less than 0.05 were obtained. Therefore, significant differences were found between at least one pair of configurations for each green hydrogen production scenario. Then, a multiple comparison test after Kruskal–Wallis between samples was performed to identify which configurations were different, with pairwise comparisons adjusted appropriately for multiple comparisons. The upper triangular part of Table 17 shows the results of the multiple comparisons test for the configurations employing the scatter search method. Again, in each cell, three letters can be seen that vary between T (true) and F (false). These refer to the green hydrogen demand scenarios of 100, 200, and 300 kg per day, respectively. It can be seen that the multiple comparisons test provided non-significant differences among the performances of configurations SS5, SS6, SS8 and SS9 in all scenarios. Furthermore, the SS3 configuration only differed from the SS6 configuration in the third scenario.

Table 17. Multiple and pairwise comparisons (SS).

			SS2	SS3	SS4	SS5	SS6	SS7	SS8	SS9	
SS2	↑↑↑		TTF	TTT	FFF	TTT	TTT	FFF	TTT	TTT	SS1
SS3	↑↑↑	↑↑=		FTF	TFF	FFF	FTT	TFF	FFF	FFT	SS2
SS4	===	↓↓↓	↓↓↓		TTF	FFF	FFT	TTF	FFF	FFF	SS3
SS5	↑↑↑	==↑	↓↓=	↑↑↑		TTT	TTT	FFF	TTT	TTT	SS4
SS6	↑↑↑	↑↑↑	==↑	↑↑↑	↑↑↑		FFF	TTT	FFF	FFF	SS5
SS7	===	↓↓↑	↓↓↓	↑==	↓↓↑	↓↓↓		TTT	FFF	FFF	SS6
SS8	↑↑↑	==↑	↓↓=	↑↑↑	===	↓↓↓	↑↑↑		TTT	TTT	SS7
SS9	↑↑↑	=↑↑	↓↓↑	↑↑↑	=↑↑	↓↓=	↑↑↑	=↑↑		FFF	SS8
	SS1	SS2	SS3	SS4	SS5	SS6	SS7	SS8			

Once significant differences had been found from the multiple comparisons test, the appropriate test for pairwise comparisons was used. The lower triangular part of Table 17 shows the results of pairwise comparisons (columns vs. rows) between the configurations

of the scatter search (SS) method. Again, in each cell, three symbols can be seen. They refer to demands of 100, 200, and 300 kg of green hydrogen per day, respectively.

As an example, pairwise comparisons between the SS6 configuration and the others can be seen. In general, the SS6 configuration outperformed the other configurations in all scenarios, except in the first and second scenarios of configuration SS3 and in the third scenario of configuration SS9, where non-significant differences were obtained. Due to the fact that the problem to be solved was to minimize, configuration SS6 provided a clear advantage, followed closely by configurations SS3 and SS9.

5. Discussion

Once the performances of the methods had been analyzed individually, a global study of comparisons between the scatter search and the other methods was developed. The complete results of this analysis are shown in Tables 18 and 19. The procedure carried out followed the steps described above.

Table 18. Multiple comparison of SS and DE (upper triangular matrix) and SS and GA (lower triangular matrix).

	SS1	SS2	SS3	SS4	SS5	SS6	SS7	SS8	SS9	DE1	DE2	DE3	DE4	DE5	DE6	DE7	DE8	DE9	
SS1		TFF	TTF	FFF	TTT	TTT	FFF	TTT	TTT	TTT	TTT	TTT	TTF	TTT	TTT	FTF	FTF	FTF	SS1
SS2	TFF		FTF	TFF	FFF	FTT	TFF	FFF	FFT	TTF	TTT	TTT	FFF	FFF	FFF	FFF	FFF	FFF	SS2
SS3	TTT	FTF		TTT	FFF	FFT	TTT	FFF	FFT	FFF	FFF	FFF	FFF	FFF	TFF	TFF	TFF	TFF	SS3
SS4	FFF	TFF	TTT		TTT	TTT	FFF	TTT	TTT	TTT	TTT	TTF	TTT	TTT	TTT	FTF	FTF	FTF	SS4
SS5	TTT	FFF	FFF	TTT		FTF	TTT	FFF	FFF	FTF	FTF	FTF	FFF	FFF	FFF	FFT	FFF	FFF	SS5
SS6	TTT	FTT	FFT	TTT	FTF		TTT	FFF	FFF	FFF	FFF	FFF	FFT	FFT	TFT	TFT	TFT	TTT	SS6
SS7	FFF	TFF	TTT	FFF	TTT	TTT		TTT	TTT	TTT	TTT	TTT	TTF	TTT	TTT	FTF	FTF	FTF	SS7
SS8	TTT	FFF	FFF	TTT	FFF	FFF	TTT		FFF	FTF	FTF	FTF	FFF	FFF	FFF	FFT	FFF	FFF	SS8
SS9	TTT	FTT	FFT	TTT	FFF	FFF	TTT	FFF		TFF	TTF	TTF	FFF	FFF	FFF	FFT	FFT	FFT	SS9
GA1	FTF	FFF	TTF	FFF	TFT	TTT	FFF	FFT	TFT		FFF	FFF	FTF	FFF	TFF	TTF	TTF	TTF	DE1
GA2	TTF	FFF	TFF	TTF	FFF	TFT	FTF	FFF	FFT	FFF		FFF	FTT	FTF	TTF	TTT	TTT	TTT	DE2
GA3	TTT	FFF	FFF	TTT	FFF	FFT	TTT	FFF	FFT	FFF	FFF		FTT	FTT	TTF	TTT	TTT	TTT	DE3
GA4	TTF	FFF	TFF	TTF	FFF	TFT	FTF	FFF	FFT	FFF	FFF	FFF		FFF	FFF	FFF	FFF	TFF	DE4
GA5	TTF	FTF	TFF	TTT	FFF	TFT	TTF	FFF	FFT	FFF	FFF	FFF	FFF		FFF	FFF	FFF	TFF	DE5
GA6	TTT	FTF	FFF	TTT	FFF	FFF	TTT	FFF	FFF	TTT	FFF	FFF	FFF	FFF		FFF	FFF	FFF	DE6
GA7	TTF	FFF	TFF	TTF	FFF	TFT	FTF	FFF	FFT	FFF	FFF	FFF	FFF	FFF	FFF		FFF	FFF	DE7
GA8	TTT	FTF	FFF	TTT	FFF	FFT	TTT	FFF	FFF	FTF	FFF	FFF	FFF	FFF	FFF	FFF		FFF	DE8
GA9	TTT	FTF	FFF	TTT	FFF	TFF	TTT	FFF	FFF	FTF	FFF	FFF	FFF	FFF	FFF	FFF	FFF		
	SS1	SS2	SS3	SS4	SS5	SS6	SS7	SS8	SS9	GA1	GA2	GA3	GA4	GA5	GA6	GA7	GA8		

Table 19. Multiple comparisons of SS and OFA.

SS1	SS2	SS3	SS4	SS5	SS6	SS7	SS8	SS9	OFA1	OFA2	OFA3	
	TTF	TTF	FFF	TTT	TTT	FFF	TTT	TTT	FFF	FFF	FFF	SS1
		FFF	TFF	FFF	FTT	FTF	FFF	FFT	TTF	TTF	TTF	SS2
			TTF	FFF	FFF	TTF	FFF	FFF	TTT	TTT	TTT	SS3
				TTT	TTT	FFF	TTT	TTT	FFF	FFF	FFF	SS4
					FFF	TTT	FFF	FFF	TTT	TTT	TTT	SS5
						TTT	FFF	FFF	TTT	TTT	TTT	SS6
							TTT	FTT	TFF	FFF	FFF	SS7
								FFF	TTT	TTT	TTT	SS8
									TTT	TTT	TTT	SS9
										FFF	FFF	OFA1
											FFF	OFA2

The upper triangular part of Table 18 shows the results of the multiple comparisons test after Kruskal–Wallis for the configurations employing both the differential evolution (DE1 to DE9) and scatter search (SS1 to SS9) methods. It can be seen that non-significant differences were found between configurations DE1-SS3, DE1-SS6, DE2-SS3, DE2-SS6 and DE3-SS6 in all scenarios. The lower triangular part of Table 18 shows the results of the multiple comparisons test after Kruskal–Wallis for the configurations employing both the

genetic algorithm (GA1 to GA9) and scatter search (SS1 to SS9) methods. It can be seen that non-significant differences were found between the pairs of configurations GA6-SS6 and GAI-SSj, with $i \in \{6, 8, 9\}$ and $j \in \{3, 5, 8, 9\}$, in all scenarios. However, significant differences were found between configurations GA8-SS6 in the third scenario and GA9-SS6 in the first scenario. Table 19 shows the results of the multiple comparisons test after Kruskal–Wallis for the configurations employing both the optimal foraging algorithm (OFA1 to OFA3) and scatter search (SS1 to SS9) methods. It can be seen that significant differences were found between the pairs of configurations involving SS3, SS6, and SS9, and the three cases of OFA.

Table 20 shows the result of the Mann–Whitney test for pairwise comparisons. In general, the configuration SS3 outperformed the configurations DE4 to DE9 in the first and second scenarios, and non-significant differences were found in the third scenario. Furthermore, the configuration SS6 outperformed configurations DE4 to DE9 in almost all scenarios (only in one case were non-significant differences found). Configuration SS6 behaved similarly to DE1 to DE3 in the first scenario, in which a demand of 100 kg of green hydrogen per day was scheduled. Regarding the second scenario, in which a demand of 200 kg of green hydrogen per day was scheduled, it can be seen that configurations DE1 to DE3 outperformed configuration SS6. Finally, it can be seen that configuration SS6 outperformed configurations DE1 to DE3 in the third scenario, in which a demand of 300 kg of green hydrogen per day was scheduled.

Regarding the genetic algorithm, configuration SS6 outperformed configurations GA1 to GA4 in all scenarios and GA5 to GA9 in the first and second scenario. Non-significant differences were found in the second scenario in relation to configurations GA5 to GA9. In addition, configurations SS3 and SS9 showed good performance. Finally, scatter search outperformed the optimal foraging algorithm in general terms. Such a circumstance brings to the light the no-free-lunch theorem [56], which states that any elevated performance for one class of problems is offset by the performance for another class for any algorithm.

Table 20. Global pairwise comparisons.

	SS1	SS2	SS3	SS4	SS5	SS6	SS7	SS8	SS9
DE1	↑↑↑	↑↑↑	=↑=	↑↑↑	↑↑=	=↑↓	↑↑↑	↑↑=	↑↑↓
DE2	↑↑↑	↑↑↑	=↑=	↑↑↑	↑↑=	=↑↓	↑↑↑	↑↑=	↑↑↓
DE3	↑↑↑	↑↑↑	=↑↑	↑↑↑	↑↑↑	=↑↓	↑↑↑	↑↑=	↑↑=
DE4	↑↑↑	=↑=	↓↓=	↑↑↑	=↑↓	↓↓↓	↑↑↑	==↓	=↓↓
DE5	↑↑↑	=↑=	↓↓=	↑↑↑	=↑↓	↓↓↓	↑↑↑	==↓	==↓
DE6	↑↑↑	=↑=	↓↓=	↑↑↑	=↑↓	↓↓↓	↑↑↑	==↓	==↓
DE7	↑↑↑	=↑=	↓↓=	↑↑↑	↓=↓	↓↓↓	↑↑↑	==↓	↓↓↓
DE8	↑↑↑	=↑=	↓↓=	↑↑↑	↓=↓	↓↓↓	↑↑↑	==↓	↓↓↓
DE9	↑↑↑	↓↑=	↓↓=	↑↑↑	↓=↓	↓↓↓	↑↑↑	==↓	↓↓↓
GA1	↑↑↑	↓↑=	↓↓=	↑↑↑	↓=↓	↓↓↓	↑↑↑	==↓	↓↓↓
GA2	↑↑↑	=↑=	↓↓=	↑↑↑	=↑↓	↓↓↓	↑↑↑	==↓	↓=↓
GA3	↑↑↑	=↑=	↓↓=	↑↑↑	=↑↓	↓↓↓	↑↑↑	==↓	↓=↓
GA4	↑↑↑	=↑=	↓↓=	↑↑↑	==↓	↓↓↓	↑↑↑	==↓	↓=↓
GA5	↑↑↑	=↑=	↓↓=	↑↑↑	=↑↓	↓=↓	↑↑↑	==↓	↓=↓
GA6	↑↑↑	=↑↑	↓==	↑↑↑	=↑↓	↓=↓	↑↑↑	=↑=	↓=↓
GA7	↑↑↑	=↑=	↓==	↑↑↑	=↑↓	↓=↓	↑↑↑	==↓	↓=↓
GA8	↑↑↑	=↑=	↓==	↑↑↑	=↑↓	↓=↓	↑↑↑	=↑↓	↓=↓
GA9	↑↑↑	=↑=	↓==	↑↑↑	=↑↓	↓=↓	↑↑↑	=↑=	↓=↓
OFA1	↓==	↓↓↓	↓↓↓	↓==	↓↓↓	↓↓↓	↓==	↓↓↓	↓↓↓
OFA2	↓==	↓↓↓	↓↓↓	↓==	↓↓↓	↓↓↓	↓==	↓↓↓	↓↓↓
OFA3	↓==	↓↓↓	↓↓↓	↓==	↓↓↓	↓↓↓	↓==	↓↓↓	↓↓↓

Having established that the most favorable configurations were DE3 for the differential evolution method, and GA6, GA8, and GA9 for the genetic algorithm, and that non-significant differences were found for the optimal foraging algorithm and SS6 for the proposed version of the scatter search method, a thorough analysis must be carried out. Tables 21–24 provide some details about the best solutions provided by the configurations for each scenario, respectively.

Table 21. Best design when DE was employed.

Conf.	H2	Pop.	CR	F	Eval.	OF	EC	Sales (MWh)	Dump (kWh)	Solution
DE3	100	50	0.9	0.9	9440	−1.9573	0.2689	27.4	510.1	4641 7 690 1
DE3	200	50	0.9	0.9	7111	−1.2655	0.4981	27.1	951.5	7244 7 1529 1
DE3	300	50	0.9	0.9	7777	0.96181	0.9383	26.2	2641.1	10,358 7 2066 2

Table 22. Best design when GA was employed.

Conf.	H2	Pop.	PrC	disC	Eval.	OF	EC	Sales (MWh)	Dump (kWh)	Solution
GA6	100	100	1.5	20	5651	−1.9573	0.2689	27.4	510.1	4641 7 690 1
GA6	200	100	1.5	20	12,251	−1.2655	0.4981	27.1	951.5	7244 7 1529 1
GA6	300	100	1.5	20	5601	0.96196	0.9380	26.2	2641.5	10,359 7 2065 2

Table 23. Best design when OFA was employed.

Conf.	H2	Pop.	Eval.	OF	EC	Sales (MWh)	Dump (kWh)	Solution
OFA1	100	50	14,301	−1.9544	0.2725	27.2	492.6	4456 7 707 1
OFA2	200	100	12,401	−1.2548	0.5041	27.1	955.6	7242 7 1555 1
OFA2	300	100	13,351	0.97640	0.9588	26.1	2633.4	10,334 7 2099 2

Table 24. Best design when SS was employed.

Conf.	H2	Pop.	Best	Diverse	Eval.	OF	EC	Sales (MWh)	Dump (kWh)	Solution
SS6	100	100	15	5	272	−1.9573	0.2689	27.4	510.1	4641 7 690 1
SS6	200	100	15	5	188	−1.2655	0.4981	27.1	951.5	7244 7 1529 1
SS6	300	100	15	5	104	0.96181	0.9383	26.2	2641.1	10,358 7 2066 2

The first columns give information regarding the method configuration and scenario solved. Next, the average number of evaluations (Eval.) of the objective function until obtaining its best value (minimum objective function value in 31 simulations) is shown. Furthermore, detailed information about the best solution provided by the configurations is displayed. This consists of the value of the objective function (OF), the energy cost (EC), the energy delivered to the grid (Sales), and the energy dumped due to the fact that the grid could not absorb it. Finally, the design for the best solution is provided. It can be seen that the average number of evaluations needed to solve the problem was 9440, 7111, and 7777 for demands of 100, 200, and 300 kg of green hydrogen per day, respectively. As an example, for a demand of 100 kg per day, the best value of the objective function in 31 simulations was −1.9573, with a energy cost of 0.2689 €/kWh. The energy supplied to the grid was around 27 MWh and the wasted energy was around 510 kWh. The design consisted of 4641 solar photovoltaic modules, seven wind turbines, a 690 kW electrolyzer, and a battery with one hour of autonomy.

With respect to SS6, it can be seen that identical solutions were obtained in each scenario regarding DE3. Nevertheless, it can be seen that the average number of evaluations needed to solve the problem was 272, 188, and 104 for demands of 100, 200, and 300 kg of green hydrogen per day, respectively. This brings to light a notable advantage over the use of many evolutionary algorithms, which require costly computing times. In particular, the use of scatter search improved the computational cost in relation to differential evolution by percentages of around 97% in all scenarios. This aspect may be very relevant, depending on the scope of the real-world problem to be solved.

In relation to the value of the objective function, it can be seen that the solution provided by DE and SS was slightly better than the solution provided by GA in the third scenario. In addition, OFA provided values of the objective function close to those provided by DE and SS but slightly larger.

6. Conclusions

This paper addressed the problem of the optimal sizing of a hybrid renewable energy system for scheduling daily green hydrogen production. Several hydrogen demand scenarios were taken into account to provide the appropriate sizing of the system. External factors related to the location of the project were considered, such as the weather conditions and the grid connection under constraints set by the energy market. As an optimization method, this paper proposed the use of scatter search, which had not previously been used to solve this problem. The results of the optimization were compared with the well-known differential evolution and genetic algorithm methods, which are a state-of-the-art evolutionary algorithms. Furthermore, the optimal foraging algorithm, which is a more recent method, was considered in the comparative study. Some configurations of the proposed modification of the scatter search method were very competitive in terms of performance. In addition, the use of scatter search outperformed the other methods in terms of computational cost, because fewer evaluations of the objective function were needed. In the case of differential evolution, the improvement was around 97%. This is promising for real-world applications that require quick responses, so the scope of analysis of the method can be extended.

From an asset management point of view, this research highlights the importance of knowing the local energy market when planning an economic investment in order to introduce a new energy system. Ignorance of the grid's limitations can lead to oversizing the installation and, therefore, to an economic investment that does not yield a return.

Some limitations of this study can be addressed in future research. From a real-world-problem point of view, larger quantities of hydrogen could be considered for production. This would allow supplying to a larger number of end-users or recovering energy for sale when the market is more favorable. This consideration requires further study of hydrogen supply to end-users and energy recovery using fuel cells. In addition, energy purchase prices were not taken into account due to their variability. This study could be extended in this respect. From an optimization point of view, a multi-objective problem has been formulated and solved as a single-objective problem. Under this approach, the objectives were aggregated into a single objective function. Therefore, a single solution was provided, which depended on the balance of the objectives in the objective function. A set of balanced solutions could be provided in case of considering a multi-objective approach. Decision-makers would have more information to make better decisions according to various limitations, such as economic or spatial constraints. In the future, the authors of the present paper will tackle the problem under a multi-objective approach by using multi-objective algorithms. Thus, each evaluation would take into account several objective functions, which is a powerful aspect of multi-objective optimization. Therefore, the current version of the single-objective scatter search method will be modified for applications within the multi-objective spectrum.

Author Contributions: Conceptualization, A.C. and J.A.M.; methodology, A.C., J.A.M. and B.G.L.; software, A.C.; validation, A.C. and J.A.M.; formal analysis, A.C. and J.A.M.; investigation, A.C., J.A.M., B.G.L., A.P. and G.W.; writing—original draft preparation, A.C. and J.A.M.; writing—review and editing, A.C., J.A.M., B.G.L., A.P. and G.W.; supervision, J.A.M., A.P. and G.W.; funding acquisition, J.A.M. and G.W. All authors have read and agreed to the published version of the manuscript.

Funding: A. Cacereño is the recipient of a postdoctoral contract from the Program “Ayudas para la recualificación del sistema universitario español para 2021-2023” (Margarita Salas) from the University of Las Palmas de Gran Canaria. This research was funded by “Ministerio de Universidades” of “Gobierno de España” (Orden UNI/501/2021, 26 May) and European Union Next Generation Funds EU.

Data Availability Statement: Dataset available on request from the authors.

Acknowledgments: A. Cacereño was welcomed in a research stance in the “Instituto Universitario de Desarrollo Regional” from the University of La Laguna (Tenerife, Spain) during 2023. The core of this research was conducted during the research stance. The authors are grateful for the support. The

authors are grateful for the support given to A. Cacereño, who is recipient of a postdoctoral contract from the Program “Ayudas para la recualificación del sistema universitario español para 2021–2023” (Margarita Salas), from the University of Las Palmas de Gran Canaria, supported by Ministerio de Universidades of Gobierno de España (Orden UNI/501/2021, 26 May) and European Union Next Generation Funds EU.

Conflicts of Interest: The authors declare no conflicts of interest.

Nomenclature

α_1	Friction coefficient
α_2	Battery bank hourly self-discharge rate
β_i	Normalization factors for the objective function
δ_T	PV maximum power temperature coefficient
η_{BAT}	Battery bank efficiency
η_{CON}	Converter efficiency
η_{ELE}	Electrolyzer efficiency
η_{INV}	Inverter efficiency
AC	Alternating current
ACC_i	Annual capital cost of the device i
ACD_i	Annualized cost of the device i
ACS	Annualized cost of the system
$AOMC_i$	Annual operation and maintenance cost of the device i
ARC_i	Annual replacement cost of the device i
C_{BAT}	Capacity of the battery bank
C_{ELE}	Capacity of the electrolyzer
CC_i	Capital cost of the device i
CON	Converter
CR	Crossover rate
CRF	Capital recovery factor
CRF_i	Capital recovery factor of the device i
D_{H_2}	Daily H ₂ demand
DC	Direct current
DE	Differential Evolution
$disC$	Distribution index of crossover
$disM$	Distribution index of polynomial mutation
EC	Energy cost
ECK	Energy consumption per kilogram of hydrogen produced
F	Scale factor
$H_2(t)$	Hydrogen production at time
H_2	Hydrogen
h_h	Height of the WT hub
h_r	Height of wind speed reference
HT_{max}	Maximum capacity of the H ₂ storage tank
$I(t)$	Solar irradiance at time
i_r	Annual rate of interest
int	Interest rate
INV	Inverter
LHHP	Lost of H ₂ production probability
LT_i	Life time of the device i
LT_{sys}	Life time of the system
M	Scaling factor of scatter search
n	Lifetime of the system
NH	Hours of battery bank autonomy
OF	Objective function

P_{BAT_0}	State of charge of the battery bank at the previous time step
P_{ELE}	Power consumption of the electrolyzer
P_{NEEDED}	Power needed to meet the energy demand of the electrolyzer
$P_{R,PV}$	PV rated power
P_{REN}	Renewable power
P_{SOLD}	Energy delivered to the grid (SALES)
P_{WT}	Wind turbine power output
PEM	Proton exchange membrane electrolyzer
PrC	Crossover probability
PrM	Mutation probability
PV	Solar photovoltaic panel
PV_N	Number of solar photovoltaic panels
$PV_p(t)$	PV expected power output
R_{REF}	Reference solar radiance
RC_i	Replacement cost of the device i
SS	Scatter Search
$T_A(t)$	Ambient temperature at time
$T_C(t)$	PV cell temperature at time
T_{NOCT}	PV cell temperature at normal operating conditions
$TNPC$	Total net present cost
U_{H_2}	Daily unmet H_2 demand
v_h	Wind speed at the height of the WT hub
v_r	Wind speed at the height of reference
$VSOC$	Virtual state of charge of the battery bank
$VSOD$	Virtual state of discharge of the battery bank
WE	Wasted energy (DUMP)
WT	Wind turbine
WT_N	Number of solar wind turbines
X	Decision variables of the problem

References

- International Energy Agency. World Energy Outlook 2022. Available online: <https://www.iea.org/reports/world-energy-outlook-2022/executive-summary> (accessed on 24 November 2024).
- Allouhi, A.; Rehman, S.; Buker, M.S.; Said, Z. Up-to-date literature review on Solar PV systems: Technology progress, market status and R&D. *J. Clean. Prod.* **2022**, *362*, 132339. [CrossRef]
- Desalegn, B.; Gebeyehu, D.; Tamirat, B. Wind energy conversion technologies and engineering approaches to enhancing wind power generation: A review. *Heliyon* **2022**, *8*, e11263. [CrossRef] [PubMed]
- Copernicus. Available online: <https://www.copernicus.eu/en> (accessed on 24 November 2024).
- Katsigiannis, Y.A.; Georgilakis, P.S.; Karapidakis, E.S. Hybrid Simulated Annealing–Tabu Search Method for Optimal Sizing of Autonomous Power Systems With Renewables. *IEEE Trans. Sustain. Energy* **2012**, *3*, 330–338. [CrossRef]
- Alshammari, N.; Asumadu, J. Optimum unit sizing of hybrid renewable energy system utilizing harmony search, Jaya and particle swarm optimization algorithms. *Sustain. Cities Soc.* **2020**, *60*, 102255. [CrossRef]
- Maleki, A.; Nazari, M.A.; Pourfayaz, F. Harmony search optimization for optimum sizing of hybrid solar schemes based on battery storage unit. *Energy Rep.* **2020**, *6*, 102–111. [CrossRef]
- Fares, D.; Fathi, M.; Mekhilef, S. Performance evaluation of metaheuristic techniques for optimal sizing of a stand-alone hybrid PV/wind/battery system. *Appl. Energy* **2022**, *305*, 117823. [CrossRef]
- He, Y.; Guo, S.; Zhou, J.; Song, G.; Kurban, A.; Wang, H. The multi-stage framework for optimal sizing and operation of hybrid electrical-thermal energy storage system. *Energy* **2022**, *245*, 123248. [CrossRef]
- Saha, S.; Saini, G.; Chauhan, A.; Upadhyay, S.; Madurai Elavarasan, R.; Hossain Lipu, M. Optimum design and techno-socio-economic analysis of a PV/biomass based hybrid energy system for a remote hilly area using discrete grey wolf optimization algorithm. *Sustain. Energy Technol. Assess.* **2023**, *57*, 103213. [CrossRef]
- Fan, X.; Liu, B.; Liu, J.; Ding, J.; Han, X.; Deng, Y.; Lv, X.; Xie, Y.; Chen, B.; Hu, W.; et al. Battery Technologies for Grid-Level Large-Scale Electrical Energy Storage. *Trans. Tianjin Univ.* **2020**, *26*, 92–103. [CrossRef]
- Khan, T.; Yu, M.; Waseem, M. Review on recent optimization strategies for hybrid renewable energy system with hydrogen technologies: State of the art, trends and future directions. *Int. J. Hydrogen Energy* **2022**, *47*, 25155–25201. [CrossRef]
- Zhang, Y.; Hua, Q.; Sun, L.; Liu, Q. Life Cycle Optimization of Renewable Energy Systems Configuration with Hybrid Battery/Hydrogen Storage: A Comparative Study. *J. Energy Storage* **2020**, *30*, 101470. [CrossRef]

14. Hosseinalizadeh, R.; Shakouri, G. H.; Amalnick, M.S.; Taghipour, P. Economic sizing of a hybrid (PV–WT–FC) renewable energy system (HRES) for stand-alone usages by an optimization-simulation model: Case study of Iran. *Renew. Sustain. Energy Rev.* **2016**, *54*, 139–150. [[CrossRef](#)]
15. Lacko, R.; Drobnič, B.; Sekavčnik, M.; Mori, M. Hydrogen energy system with renewables for isolated households: The optimal system design, numerical analysis and experimental evaluation. *Energy Build.* **2014**, *80*, 106–113. [[CrossRef](#)]
16. Das, H.S.; Tan, C.W.; Yatim, A.; Lau, K.Y. Feasibility analysis of hybrid photovoltaic/battery/fuel cell energy system for an indigenous residence in East Malaysia. *Renew. Sustain. Energy Rev.* **2017**, *76*, 1332–1347. [[CrossRef](#)]
17. Duman, A.C.; Güler, Ö. Techno-economic analysis of off-grid PV/wind/fuel cell hybrid system combinations with a comparison of regularly and seasonally occupied households. *Sustain. Cities Soc.* **2018**, *42*, 107–126. [[CrossRef](#)]
18. Mohseni, S.; Brent, A.C.; Burmester, D. A comparison of metaheuristics for the optimal capacity planning of an isolated, battery-less, hydrogen-based micro-grid. *Appl. Energy* **2020**, *259*, 114224. [[CrossRef](#)]
19. Siddiqui, O.; Dincer, I. Optimization of a new renewable energy system for producing electricity, hydrogen and ammonia. *Sustain. Energy Technol. Assess.* **2021**, *44*, 101023. [[CrossRef](#)]
20. Sun, H.; Ebadi, A.G.; Toughani, M.; Nowdeh, S.A.; Naderipour, A.; Abdullah, A. Designing framework of hybrid photovoltaic-biowaste energy system with hydrogen storage considering economic and technical indices using whale optimization algorithm. *Energy* **2022**, *238*, 121555. [[CrossRef](#)]
21. El-Sattar, H.A.; Kamel, S.; Sultan, H.M.; Zawbaa, H.M.; Jurado, F. Optimal design of Photovoltaic, Biomass, Fuel Cell, Hydrogen Tank units and Electrolyzer hybrid system for a remote area in Egypt. *Energy Rep.* **2022**, *8*, 9506–9527. [[CrossRef](#)]
22. Elnozahy, A.; Sayed, M.; Ali, A.; Nayel, M.A. Optimal Techno-economic Sizing of Electrical/Green Hydrogen Generation System for Hybrid Demand Load. In Proceedings of the 23rd International Middle East Power Systems Conference (MEPCON 2022), Cairo, Egypt, 13–15 December 2022; pp. 1–8. [[CrossRef](#)]
23. Güven, A.F.; Özdal Mengi, O. Assessing metaheuristic algorithms in determining dimensions of hybrid energy systems for isolated rural environments: Exploring renewable energy systems with hydrogen storage features. *J. Clean. Prod.* **2023**, *428*, 139339. [[CrossRef](#)]
24. Phan-Van, L.; Takano, H.; Nguyen Duc, T. A comparison of different metaheuristic optimization algorithms on hydrogen storage-based microgrid sizing. *Energy Rep.* **2023**, *9*, 542–549. [[CrossRef](#)]
25. Irham, A.; Roslan, M.; Jern, K.P.; Hannan, M.; Mahlia, T.I. Hydrogen energy storage integrated grid: A bibliometric analysis for sustainable energy production. *Int. J. Hydrogen Energy* **2024**, *63*, 1044–1087. [[CrossRef](#)]
26. García-Triviño, P.; Fernández-Ramírez, L.M.; Gil-Mena, A.J.; Llorens-Iborra, F.; García-Vázquez, C.A.; Jurado, F. Optimized operation combining costs, efficiency and lifetime of a hybrid renewable energy system with energy storage by battery and hydrogen in grid-connected applications. *Int. J. Hydrogen Energy* **2016**, *41*, 23132–23144. [[CrossRef](#)]
27. Gharibi, M.; Askarzadeh, A. Technical and economical bi-objective design of a grid-connected photovoltaic/diesel generator/fuel cell energy system. *Sustain. Cities Soc.* **2019**, *50*, 101575. [[CrossRef](#)]
28. Okundamiya, M. Size optimization of a hybrid photovoltaic/fuel cell grid connected power system including hydrogen storage. *Int. J. Hydrogen Energy* **2021**, *46*, 30539–30546. [[CrossRef](#)]
29. Le, T.S.; Nguyen, T.N.; Bui, D.K.; Ngo, T.D. Optimal sizing of renewable energy storage: A techno-economic analysis of hydrogen, battery and hybrid systems considering degradation and seasonal storage. *Appl. Energy* **2023**, *336*, 120817. [[CrossRef](#)]
30. Martí, R.; Corberán, Á.; Peiró, J. Scatter Search. In *Handbook of Heuristics*; Martí, R., Pardalos, P.M., Resende, M.G.C., Eds.; Springer International Publishing: Cham, Switzerland, 2018; pp. 717–740, ISBN 978-3-319-07124-4. [[CrossRef](#)]
31. Glover, F. Heuristics for integer programming using surrogate constraints. *Decis. Sci.* **1977**, *8*, 156–166. [[CrossRef](#)]
32. Laguna, M.; Martí, R. *Scatter Search: Methodology and Implementations in C*; Springer Science + Business Media, LLC: Berlin/Heidelberg, Germany, 2003; ISBN 978-1-4613-5027-9. [[CrossRef](#)]
33. de Athayde Costa e Silva, M.; Klein, C.E.; Mariani, V.C.; dos Santos Coelho, L. Multiobjective scatter search approach with new combination scheme applied to solve environmental/economic dispatch problem. *Energy* **2013**, *53*, 14–21. [[CrossRef](#)]
34. Tan, Y.; Zhou, M.; Zhang, Y.; Guo, X.; Qi, L.; Wang, Y. Hybrid Scatter Search Algorithm for Optimal and Energy-Efficient Steelmaking-Continuous Casting. *IEEE Trans. Autom. Sci. Eng.* **2020**, *17*, 1814–1828. [[CrossRef](#)]
35. Pérez Posada, A.F.; Villegas, J.G.; López-Lezama, J.M. A Scatter Search Heuristic for the Optimal Location, Sizing and Contract Pricing of Distributed Generation in Electric Distribution Systems. *Energies* **2017**, *10*, 1449. [[CrossRef](#)]
36. Stojiljković, M.M. Bi-level multi-objective fuzzy design optimization of energy supply systems aided by problem-specific heuristics. *Energy* **2017**, *137*, 1231–1251. [[CrossRef](#)]
37. Storn, R.; Price, K. Differential Evolution—A Simple and Efficient Heuristic for Global Optimization over Continuous Spaces. *J. Glob. Optim.* **1997**, *11*, 341–359. [[CrossRef](#)]
38. Holland, J.H. *Adaptation in Natural and Artificial Systems: An Introductory Analysis with Applications to Biology, Control, and Artificial Intelligence*; MIT Press: Cambridge, MA, USA, 1992.
39. Ramli, M.A.; Boucekara, H.; Alghamdi, A.S. Optimal sizing of PV/wind/diesel hybrid microgrid system using multi-objective self-adaptive differential evolution algorithm. *Renew. Energy* **2018**, *121*, 400–411. [[CrossRef](#)]
40. Yang, Y.; Li, R. Techno-Economic Optimization of an Off-Grid Solar/Wind/Battery Hybrid System with a Novel Multi-Objective Differential Evolution Algorithm. *Energies* **2020**, *13*, 1585. [[CrossRef](#)]

41. Abedi, S.; Ahangar, H.G.; Nick, M.; Hosseini, S.H. Economic and reliable design of a hybrid PV-wind-fuel cell energy system using differential evolutionary algorithm. In Proceedings of the 19th Iranian Conference on Electrical Engineering, Tehran, Iran, 17–19 May 2011; pp. 1–6.
42. Martí, R.; Sevaux, M.; Sörensen, K. Fifty years of metaheuristics. *Eur. J. Oper. Res.* **2025**, *321*, 345–362. [[CrossRef](#)]
43. Nagapurkar, P.; Smith, J.D. Techno-economic optimization and environmental Life Cycle Assessment (LCA) of microgrids located in the US using genetic algorithm. *Energy Convers. Manag.* **2019**, *181*, 272–291. [[CrossRef](#)]
44. Zhu, G.Y.; Zhang, W.B. Optimal foraging algorithm for global optimization. *Appl. Soft Comput.* **2017**, *51*, 294–313. [[CrossRef](#)]
45. Patel, M.R. *Wind and Solar Power Systems*; CRC Press: Boca Raton, FL, USA, 1999; ISBN 0-8493-1605-7.
46. Anoune, K.; Ghazi, M.; Bouya, M.; Laknizi, A.; Ghazouani, M.; Abdellah, A.B.; Astito, A. Optimization and techno-economic analysis of photovoltaic-wind-battery based hybrid system. *J. Energy Storage* **2020**, *32*, 101878. [[CrossRef](#)]
47. Morante, J.R.; Andreu, T.; García, G.; Guilera, J.; Tarancón, A.; Torrell, M. *Hidrógeno: Vector Energético de Una Economía Descarbonizada*, 2nd ed.; Fundación Naturgy: Madrid, Spain, 2020; ISBN 978-84-09-22546-0.
48. Sultan, H.M.; Menesy, A.S.; Kamel, S.; Korashy, A.; Almohaimed, S.; Abdel-Akher, M. An improved artificial ecosystem optimization algorithm for optimal configuration of a hybrid PV/WT/FC energy system. *Alex. Eng. J.* **2021**, *60*, 1001–1025. [[CrossRef](#)]
49. Tian, Y.; Cheng, R.; Zhang, X.; Jin, Y. PlatEMO: A MATLAB platform for evolutionary multi-objective optimization. *IEEE Comput. Intell. Mag.* **2017**, *12*, 73–87. [[CrossRef](#)]
50. Simon, D. *Evolutionary Optimization Algorithms*; John Wiley: Hoboken, NJ, USA, 2013.
51. Shapiro, S.S.; Wilk, M.B. An analysis of variance test for normality (complete samples). *Biometrika* **1965**, *52*, 591–611. [[CrossRef](#)]
52. Hollander, M.; Wolfe, D. *Nonparametric Statistical Methods*; John Wiley & Sons, Inc.: Hoboken, NJ, USA, 1973.
53. R Core Team. R: A Language and Environment for Statistical Computing. 2022. Available online: <https://www.R-project.org/> (accessed on 24 November 2024).
54. Siegel, S.; Castellan, N. *Non Parametric Statistics for the Behavioural Sciences*; MacGraw Hill: New York, NY, USA, 1988.
55. Giraudoux, P.; Antonietti, J.; Beale, C.; Groemping, U.; Lancelot, R.; Pleydell, D.; Treglia, M. pgirmess: Spatial Analysis and Data Mining for Field Ecologists. R Package Version 2.0.3. Available online: <https://CRAN.R-project.org/package=pgirmess> (accessed on 24 November 2024).
56. Wolpert, D.; Macready, W. No free lunch theorems for optimization. *IEEE Trans. Evol. Comput.* **1997**, *1*, 67–82. [[CrossRef](#)]

Disclaimer/Publisher’s Note: The statements, opinions and data contained in all publications are solely those of the individual author(s) and contributor(s) and not of MDPI and/or the editor(s). MDPI and/or the editor(s) disclaim responsibility for any injury to people or property resulting from any ideas, methods, instructions or products referred to in the content.